# Analyzing Simulated Convective Bursts in Two Atlantic Hurricanes. Part II: Intensity Change due to Bursts

ANDREW T. HAZELTON[a] AND ROBERT E. HART

*Department of Earth, Ocean and Atmospheric Science, The Florida State University, Tallahassee, Florida*

ROBERT F. ROGERS

*NOAA/AOML/Hurricane Research Division, Miami, Florida*

(Manuscript received 15 July 2016, in final form 11 April 2017)

ABSTRACT

This paper investigates convective burst (CB) evolution in Weather Research and Forecasting (WRF) Model simulations of two tropical cyclones (TCs), focusing on the relationship between CBs and TC intensity change. Analysis of intensity change in the simulations shows that there are more CBs inside the radius of maximum winds (RMW) during times when the TCs are about to intensify, while weakening/steady times are associated with more CBs outside the RMW, consistent with past observational and theoretical studies. The vertical mass flux distributions show greater vertical mass flux at upper levels both from weaker updrafts and CBs for intensifying cases. The TC simulations are further dissected by past intensity change, and times of sustained intensification have more CBs than times when the TC has been weakening but then intensifies. This result suggests that CB development may not always be predictive of intensification, but rather may occur as a result of ongoing intensification and contribute to ongoing intensification. Abrupt short-term intensification is found to be associated with an even higher density of CBs inside the RMW than is slower intensification. Lag correlations between CBs and intensity reveal a broad peak, with the CBs leading pressure falls by 0–3 h. These relationships are further confirmed by analysis of individual simulation periods, although the relationship can vary depending on environmental conditions and the previous evolution of the TC. These results show that increased convection due to both weak updrafts and CBs inside the RMW is favorable for sustained TC intensification and show many details of the typical short-term response of the TC core to CBs.

## 1. Introduction

Predicting short-term intensity change of tropical cyclones (TCs) continues to be a major operational and research challenge. Forecasting the small-scale (~5 km or less) details of physical and dynamical processes that affect intensity change on the time scale of a day or less continues to prove elusive despite the improvements to hurricane models like the Hurricane Weather Research and Forecasting (HWRF) Model (e.g., Tallapragada et al. 2014). Some of these details include TC interaction with areas of high sea surface temperature (SST) or ocean heat content (OHC) (e.g., Shay et al. 2000), TC response to shear (e.g., Reasor et al. 2013), eyewall replacement cycles (e.g., Willoughby et al. 1982; Kossin and Sitkowski 2009), eyewall instabilities (e.g., Kossin and Schubert 2001), and changes in outflow (e.g., Molinari and Vollaro 2014), among others. Hazelton et al. (2017, hereafter Part I) explored the formation of convective bursts (CBs), extreme updrafts in the TC core, and analyzed the asymmetric flow and other factors that lead to their development. These extreme, asymmetric convective features are one potential source for TC intensity change.

A recent research focus is the development of deep convection in the TC core. Recent observational and modeling studies have analyzed the importance of deep convection in TC intensity change. Hack and Schubert (1986) and Vigh and Schubert (2009) used a balanced vortex model to show that diabatic heating is favorable for TC intensification when it is located in a region of

[a] Current affiliation: Program in Atmospheric and Oceanic Science, Princeton University, and NOAA/GFDL, Princeton, New Jersey.

*Corresponding author*: Andrew Hazelton, andy.hazelton.1003@gmail.com

DOI: 10.1175/MWR-D-16-0268.1

large inner-core inertial stability. Conversely, this heating is less effective for intensification when it is located in the lower inertial stability region outside the core, in agreement with Nolan et al. (2007). However, Smith and Montgomery (2016) suggest that TC intensification is driven by boundary layer spinup of tangential winds rather than diabatic heating in the core, and the warm core responds to this spinup rather than causing intensification. This boundary layer spinup idea still relies, however, on the assumption that the bulk of the diabatic heating is inside the radius of maximum wind (RMW), that is, in the region of high inertial stability.

Steranka et al. (1986) performed one of the first observational studies to examine the impact of convection on intensity change. Their study found that TCs with a larger area of cold cloud tops in the inner-core region were more likely to strengthen compared to those with less/weaker convection. Rodgers et al. (1998) examined Hurricane Opal (1995) and found that the periods with eyewall CBs coincided with rapid deepening. Heymsfield et al. (2001) analyzed a persistent CB in the northeastern quadrant of Hurricane Bonnie (1998), and showed that some of the subsidence causing Bonnie's eye to warm was due to updraft air reaching the tropopause and sinking into the eye. Kelley et al. (2004) used Tropical Rainfall Measuring Mission (TRMM) radar data to show that tall convective towers (measured using the 20-dB$Z$ threshold) in the eyewall of a TC favors intensification. A follow-up study by Kelley et al. (2005) using WSR-88D data yielded similar results, finding that TCs with a larger frequency of tall convective towers tended to intensify more than those with fewer towers. Kelley and Halverson (2011) attempted to quantify the amount of TC intensification associated with CB development and found that a persistent (~12 h) CB could increase the amount of eyewall latent heat release by 25% and increase the tangential winds by up to 16 m s$^{-1}$, after accounting for friction.

Guimond et al. (2010) observed hot towers in the core of Hurricane Dennis (2005) preceding rapid intensification (RI) and hypothesized that the intensification of the TC during this period was due to axisymmetrization of the vorticity induced by the hot tower, as well as forced subsidence associated with the tower. Likewise, an observational study by Monette et al. (2012) identified "overshooting tops" using infrared satellite data and found that a predictor based on these features could add skill to predictions of TC RI. Rogers et al. (2013) similarly showed that intensifying TCs tended to have more CBs (there defined by the 99th percentile of positive vertical velocity, i.e., 5.5 m s$^{-1}$ at $z$ = 8 km) than steady-state TCs, especially inside the RMW. Consistent with these findings, Rogers et al. (2015) examined the RI of Hurricane Earl (2010), and found that CBs helped the vortex to become vertically stacked, initiating RI. This study also compared Earl to Gustav (which was steady state at the time of analysis), and found that Gustav had more CBs concentrated outside the RMW. Compared to Earl, Gustav also had less of a difference between updraft slope and the slope of an angular momentum surface (e.g., Stern et al. 2014), a factor found to be a signature of steady TCs by Hazelton et al. (2015). Stevenson et al. (2014) further supported the idea of convection inside the RMW leading to intensification, finding that most of the lightning inside the RMW of Earl occurred just prior to RI onset. Yet another study of Hurricane Earl, by Susca-Lopata et al. (2015), used lightning and passive microwave data to show that intense convection inside the RMW preceded the RI of Earl, consistent with the other studies. Guimond et al. (2016) showed that CBs contributed to asymmetric intensification of Hurricane Karl (2010) by strengthening the TC warm core. Finally, Rogers et al. (2016) found that deep convection was present in the core of Hurricane Edouard (2014), particularly in the upshear-left quadrant, during an intensification period. Together, all of these studies indicate that strong eyewall convection can be associated with intensification, particularly when that convection is inside the RMW where the heating can be more efficiently retained.

Numerical studies have also investigated the relationship between eyewall convection and intensity change. Rogers (2010) analyzed the evolution of convection and precipitation in Hurricane Dennis (2005) using an MM5 simulation, and found that there was an increase in the vertical mass flux from CBs 6–12 h prior to RI. This study, however, found that the biggest precursor to RI was the coverage of weaker updrafts. Fierro and Reisner (2011) found that the pressure in a simulation of Hurricane Rita fell quickly after an episode of strong vertical motion and lightning in the eyewall. McFarquhar et al. (2012) also performed a WRF simulation of Hurricane Dennis and found that the extreme outliers of the vertical velocity distribution ($w$ = 20–24 m s$^{-1}$) preceded the onset of RI, while the coverage of and impacts from slightly weaker bursts occurred during and after RI onset. Chen and Zhang (2013) performed a WRF simulation of Hurricane Wilma (2005) and showed that CBs preceded RI. They found that the heating induced by the bursts well before RI tended to propagate away from the core with gravity waves, and that the heating became more efficient after a cyclonic circulation formed aloft in the inner core. Chen and Gopalakrishnan (2015) simulated

Hurricane Earl using HWRF, and again found that inner-core CBs preceded the initial RI. However, that study specifically found that convection in the downshear-left and upshear-left quadrants was key to the initiation of RI, since the compensating subsidence could create warming in the upshear region before being advected over the storm center, leading to pressure falls. Kanada and Wada (2015) performed a simulation of Typhoon Ida (1958), and again found that CBs were associated with RI of the typhoon. These studies indicate that strong eyewall convection can be associated with intensification, particularly when that convection occurs inside the RMW.

While these studies have clearly shown that strong convection is associated with intensification, there is some disagreement as to the timing of strong convection in relation to intensity change. For example, Cecil et al. (2010) used ER-2 radar observations of Hurricane Emily (2005) to note that there was an area of strong convection in the eyewall several hours after the storm had begun a weakening period. DeMaria et al. (2012) found that inner-core cloud-to-ground lightning was actually more of a signal for TC weakening than intensification. Jiang (2012) found, using TRMM data, that there were differences in convective intensity between intensifying and weakening TCs, but the probability of RI was not significantly increased for cases with convective bursts (referred to as hot towers in that study) in the inner core. Jiang and Ramirez (2013) used TRMM data to show that RI was not always associated with deeper convection than slowly intensifying or weakening storms, and Zagrodnik and Jiang (2014) found that deep convection did not precede RI, but rather occurred after RI onset. These disagreements about timing illustrate the need for further investigation.

The prior work shows ample evidence for convection in the inner core being a precursor of intensification, including RI. However, there are differences among the studies related to the timing of intensity change relative to CB development, including whether CBs are most prominent before intensification begins or when intensification is ongoing. There are also disagreements in the literature about the relative role of weak updrafts and extreme updrafts, and which contribute to intensity change. In addition, the time scale of the intensity response is somewhat unclear from these studies. These disagreements and questions will be addressed by analyzing numerical model output for two TCs with both intensification and weakening periods, to assess the intensity response to CBs within a high-resolution framework.

The next section briefly revisits the method used to calculate convective burst development in the simulations, and describes the general distribution of CBs in the simulations. The results section begins by analyzing CB distributions stratified by intensity change and then examines lag correlations between CBs and intensity change. The results section concludes with an analysis of key time periods in each simulation where significant CB activity and/or intensity change occur. Finally, the conclusions of the study and physical implications are discussed.

## 2. Data and methodology

Part I of this study described the WRF-ARW simulations (at 2-km horizontal grid spacing) of Hurricanes Dean (2007) and Bill (2009), and their success at producing many of the observed track and intensity fluctuations, including periods of abrupt short-term intensification [defined later as pressure falls of at least 3 hPa $(3\,\mathrm{h})^{-1}$], steady intensification [pressure falls between 0.5 and 3 hPa $(3\,\mathrm{h})^{-1}$], and weakening (3-h pressure rises). Part I also described the methodology used to identify CBs in each simulation, based on the 99th percentile of the mean vertical velocity in the 6–12-km layer in each simulation. This study extends Part I by examining the intensity response to the most extreme updrafts, not necessarily the entire spectrum of TC updrafts. Figures 1a and 1b show time series of intensity as well as CB counts inside and outside the 6–12-km layer-averaged RMW (hereafter $\mathrm{RMW}_{6\text{–}12}$) after the spinup period for each simulation. The times when shear increased in each simulation (see Fig. 1 of Part I) are shown in the figures, along with a possible eyewall replacement cycle (ERC) beginning in the Dean simulation. Spikes in CB activity inside $\mathrm{RMW}_{6\text{–}12}$ can be seen during each of the intensification periods for Dean and Bill, with generally less activity during most of the weakening/steady periods. Figures 1c and 1d show the azimuthal mean heating rate ($\partial\theta/\partial t$) over the time period of the simulation (with a 3-h running mean applied to smooth the data), averaged in and just inside the eyewall region from $0.5\mathrm{RMW}_3$ to $\mathrm{RMW}_3$. It should be noted that this heating rate includes all potential sources (e.g., convective heating as well as other possible factors such as advection). The periods of heating for Dean occur during or after the spikes in CB counts inside $\mathrm{RMW}_{6\text{–}12}$, with little change or cooling occurring when CBs were primarily outside $\mathrm{RMW}_{6\text{–}12}$. This difference between CBs inside and outside the $\mathrm{RMW}_{6\text{–}12}$ also seems to be connected to the intensity change, and this difference will be quantified in detail throughout the study.

Figure 3 in Part I, showing the distribution of CBs in a shear-relative sense, is reproduced here as Fig. 2. As mentioned in Part I, the CB locations were calculated in normalized radius–azimuth coordinates, and then interpolated to a normalized Cartesian coordinate system for the density plots. The densities are then

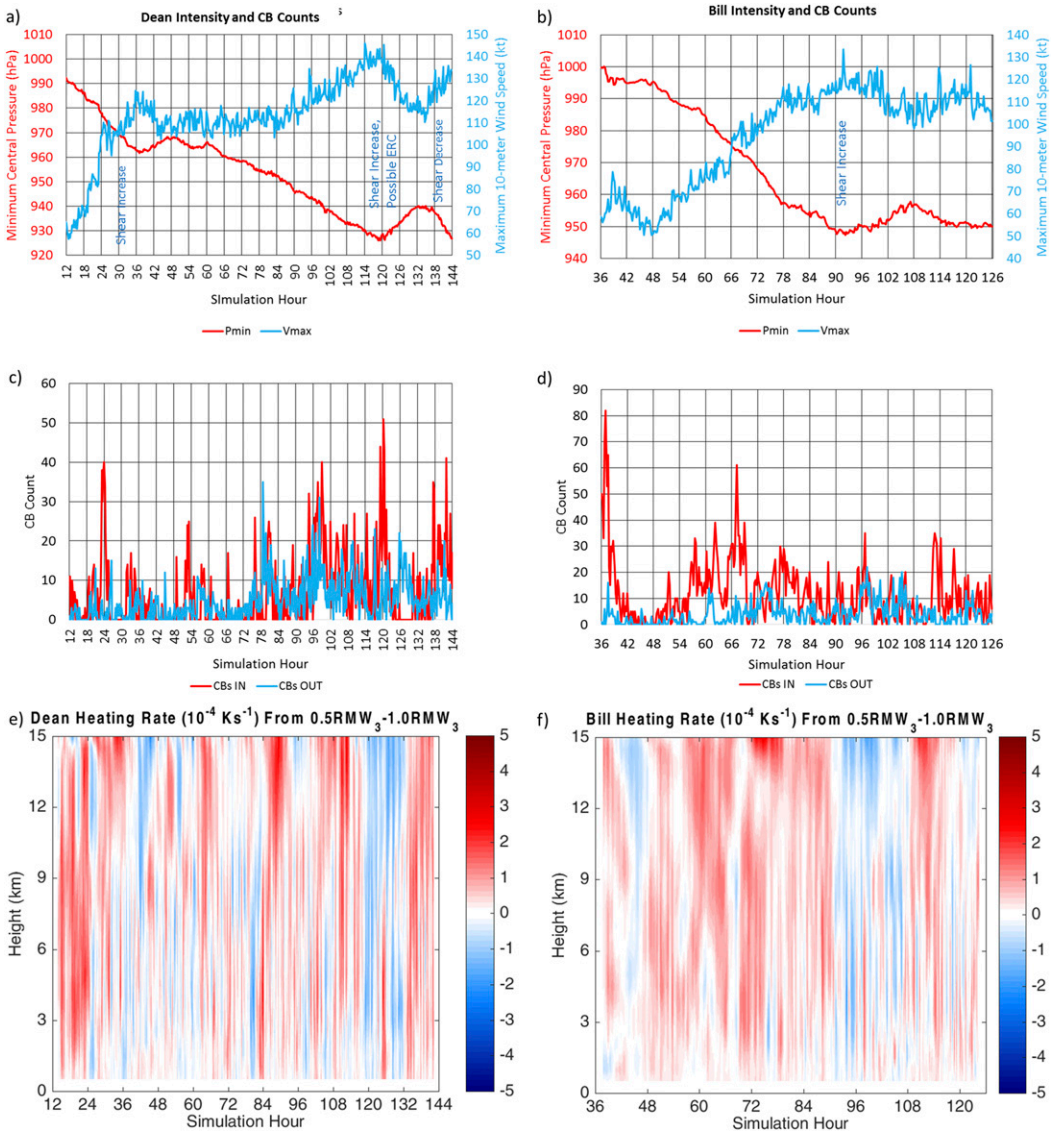


FIG. 1. (a) Time series of minimum pressure (hPa, red) and maximum wind speed (kt, blue) for the Dean simulation. Periods of increasing shear as well as the beginning of a possible ERC are shown. (b) As in (a), but for the Bill simulation. (c) Time series of CB counts inside the 6–12-km mean RMW (red) and outside the 6–12-km mean RMW (blue) for the Dean simulation. (d) As in (c), but for the Bill simulation. (e) Time evolution of the heating rate ($\partial\theta/\partial t$), azimuthally averaged and averaged inside and near the eyewall (from 0.5RMW$_3$ to RMW$_3$), for the Dean simulation. A 3-h running mean has been applied. (f) As in (e), but for the Bill simulation.

binned every $0.1X/\mathrm{RMW}_{6\text{–}12} \times 0.1Y/\mathrm{RMW}_{6\text{–}12}$ (essentially a two-dimensional histogram), normalized by the number of times from each simulation. For both TC simulations, the highest density of CBs is in the downshear region, particularly in the downshear-left (DSL) quadrant. As mentioned in Part I, this result is consistent with prior work analyzing shear-relative distributions of convective activity in TCs (e.g., Black et al. 2002; Corbosiero and Molinari 2002; Rogers et al. 2013; Reasor et al. 2013; DeHart et al. 2014).

## 3. Results

### a. *CB distributions separated by intensity change*

#### 1) INTENSIFYING VERSUS WEAKENING/STEADY CASES

Because of the more transient nature of the wind maxima and the higher reliability and confidence in pressure measurements in the observations (e.g., Knaff and Zehr 2007), the intensity metric used throughout the

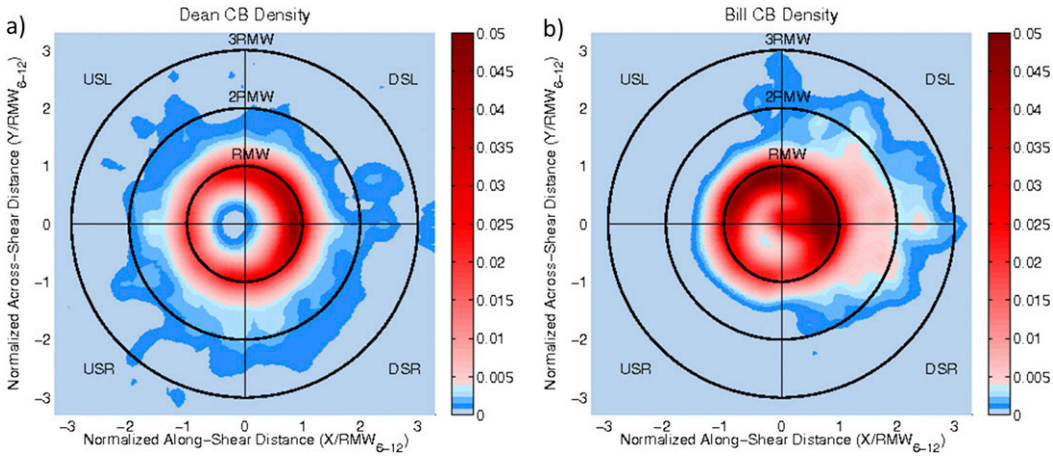


FIG. 2. (a) Density (count per normalized 0.1 × 0.1 grid point, per simulation time) of convective bursts in the Dean simulation (calculated by binning all of the CBs from Dean after spinup). The horizontal coordinate system is normalized by the 6–12-km mean RMW, and also rotated relative to the 850–200-hPa shear vector. The counts are normalized by the number of cases in each simulation. (b) As in (a), but for the Bill simulation.

study is the minimum surface pressure, the evolution of which is shown in Fig. 1. The intensity of a TC can evolve on a variety of time scales, but for the initial analysis of intensity change, the results are stratified by 3-h intensity change, with the 3-h periods initiated every 15 min of model output. This time scale is long enough to avoid short-term very small intensity fluctuations but also short enough to improve on the coarser 12-h resolution used in prior observational studies, such as by Rogers et al. (2013). The intensity change was calculated by forward differencing over the 3-h period ("forward intensity change"). Later, backward differencing ("backward intensity change") will be discussed. Intensifying time periods were defined by the requirement that the 3-h pressure fall be greater than 0.5 hPa, in order to avoid very small-scale fluctuations ;such as the diurnal cycle; e.g., Dunion et al. (2014)] that are not truly representative of an intensifying TC. The "intensifying" times include both persistent, gradual intensification as well as rapid intensification for this initial comparison. The weakening/steady times were defined as those with a pressure rise in the forward 3 h, or those where the pressure remained constant. Because of the smaller sample size of the weakening/steady times and the inclusion of the steady-state times with the weakening times, the 0.5 hPa $(3\,\mathrm{h})^{-1}$ threshold was not applied to the weakening/steady cases.

Figure 3 shows the density of CBs in a shear-relative, RMW-normalized coordinate system for the intensifying and weakening/steady groups for both simulations. Once again, the counts have been scaled by the sample size in each group, to allow for direct comparison. There are more CBs inside $\mathrm{RMW}_{6\text{–}12}$ for the intensifying times for both Dean and Bill. Interestingly, the density is actually higher upshear left (USL) for weakening/steady periods for Bill than intensifying, which appears to contradict recent results about the importance of upshear convection to intensification [e.g., Rogers et al. (2016) in a study of Hurricane Edouard]. However, the higher density of CBs well outside $\mathrm{RMW}_{6\text{–}12}$ for these weakening/steady times (for both Dean and Bill) is consistent with the idea that convection outside the RMW tends to lead to steady-state or weakening periods. Notice that the CBs outside $\mathrm{RMW}_{6\text{–}12}$ are almost all confined to the downshear region in the Bill simulation, indicative of a heightened influence of deep-layer shear (e.g., Braun and Wu 2007).

To assess the statistical significance of these results, the mean and median of the CB counts inside and outside $\mathrm{RMW}_{6\text{–}12}$ are calculated for the intensifying and weakening/steady groups for both simulations, and the significance is analyzed using a Wilcoxon rank-sum test. The results are summarized in Tables 1 and 2. The higher CB counts inside $\mathrm{RMW}_{6\text{–}12}$ for intensifying cases versus weakening/steady cases are statistically significant. Interestingly, the higher counts outside $\mathrm{RMW}_{6\text{–}12}$ for weakening/steady cases (compared to intensifying) show up for both simulations, but are only significant for Bill. However, the difference between counts inside and outside is larger for intensifying cases in both simulations, and is statistically significant for both. Overall, these results are consistent with the findings of the composite radar study of Rogers et al. (2013), which found that intensifying TCs had more CBs inside the RMW, while steady-state TCs had more CBs outside. This finding is also consistent with case studies of

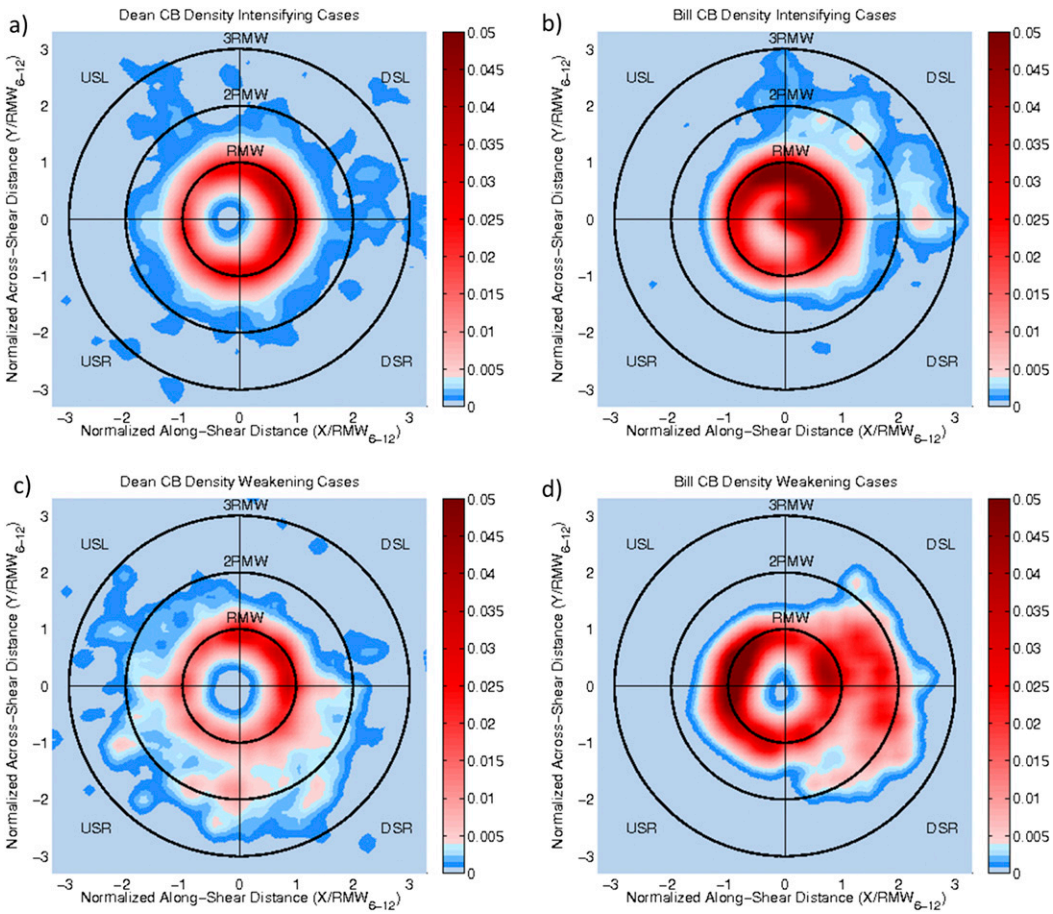


FIG. 3. (a) Density of CBs in the Dean simulation prior to intensifying time periods. (b) As in (a), but for the Bill simulation. (c) Density of CBs in the Dean simulation prior to weakening/steady time periods. (d) As in (c), but for the Bill simulation. Once again, the horizontal coordinate system is normalized by the 6–12-km mean RMW, and also rotated relative to the 850–200-hPa shear vector. The densities are again normalized by the sample size in each group.

Hurricane Earl (2010) by Stevenson et al. (2014), Rogers et al. (2015), and Susca-Lopata et al. (2015).

To examine the full spectrum of vertical velocity in relation to intensity change, and to provide context for the further examination of CBs, the contributions to the total vertical mass flux by updrafts of different magnitudes were examined. This was done by creating contoured frequency by altitude diagrams (CFADs) of the vertical mass flux as a function of vertical velocity for the intensifying and weakening cases in each simulation, as well as a difference CFAD for each case. The vertical mass flux was normalized by the maximum value in a single vertical velocity–height bin, after Rogers et al. (2013). Only vertical velocities within the eyewall region (defined as $0.75\mathrm{RMW}_3$–$1.50\mathrm{RMW}_3$) were included.

The results of the mass flux calculations are shown in Fig. 4. As in Rogers (2010) and Rogers et al. (2013), the updraft mass flux is dominated by weaker updrafts

TABLE 1. Comparison of CB counts (per model output time) inside and outside the RMW, as well as the difference between the counts inside and outside (per model time), for the Dean WRF simulation for times when the TC intensified (IN) in the 3 h after the bursts were observed vs times that the TC weakened or remained steady (WS). Statistical relationships between the categories are also quantified. Relationships significant at the 90% level are italicized, relationships significant at the 95% level are set in boldface, and relationships significant at the 99% level are boldface and italicized.

| | CBs inside RMW | CBs outside RMW | Difference |
|---|---|---|---|
| IN Mean (median) | 7.0 (4) | 4.8 (3) | 2.2 (0) |
| WS Mean (median) | 4.5 (0) | 5.3 (4) | −0.8 (0) |
| Rank-sum test results ($p$ value) | ***IN*** > ***WS*** ($p < 0.01$) | IN = WS ($p = 0.20$) | ***IN*** > ***WS*** ($p < 0.01$) |

TABLE 2. As in Table 1, but for the Bill simulation.

| | CBs inside RMW | CBs outside RMW | Difference |
|---|---|---|---|
| IN Mean (median) | 12.6 (10) | 3.1 (2) | 9.5 (6) |
| WS Mean (median) | 8.7 (7) | 7.4 (6) | 1.3 (2) |
| Rank-sum test results ($p$ value) | **IN** > **WS** ($p = 0.04$) | ***IN*** < ***WS*** ($p < 0.01$) | ***IN*** > ***WS*** ($p < 0.01$) |

(0–2 m s$^{-1}$) below 3-km height for both intensifying and weakening cases. The largest differences in updraft mass flux between weakening and intensifying cases are found in the vertical extent of the weak updrafts above ~9 km, which is different from the results of Rogers (2010), where the primary difference was found at lower levels (below ~1.5 km). For both TCs, there is also a broader area of greater mass flux in the 5–10-km height range for the intensifying cases accomplished by extreme updrafts (about 5–15 m s$^{-1}$ for Dean and 5–10 m s$^{-1}$ for Bill). This finding is consistent with the results of Rogers et al. (2013), and these vertical velocity ranges correspond relatively closely with the CB thresholds for each case. Interestingly, the Dean cases do now show a major intensifying–weakening difference in downdrafts, but for Bill the weakening cases had much greater downdraft mass flux, likely related to the stronger shear and associated vertical motion asymmetries. The mass flux distributions suggest that both weaker and extreme updrafts at upper levels can help to distinguish between intensifying and weakening in the short term. While the relative importance of weaker and more extreme updrafts in distinguishing TC intensification is a topic worthy of continued investigation, the rest of this study will focus in particular on the contribution from the extreme updrafts (CBs).

### 2) ABRUPT SHORT-TERM INTENSIFICATION VERSUS SLOW INTENSIFICATION

Next, the CB distributions prior to rapid short-term intensification [called abrupt short-term intensification (ASI)] are calculated. ASI cases are defined as times where the pressure fell at least 3 hPa in the forward 3-h period used to define intensity change. This short-term intensity change metric is different than the time scale typically used to define RI [24 h; e.g., Kaplan et al. (2010)], since, as will be seen later, CB impacts on intensity change seem to occur on approximately this time scale. It should be noted that such a definition will potentially include times where the storm briefly undergoes ASI but the intensification is not sustained for 24-h RI. The ASI times were compared with the times when the storm was intensifying, but at a persistent, slower rate [SI, between 0.5 and 3 hPa (3 h)$^{-1}$]. For Dean, the ASI times are ~32% of the total intensifying times. However, for Bill, the ASI times are only ~12% of the total intensifying times. Figure 5 shows the CB densities for the ASI and SI times, with the counts again normalized based on sample size. For Dean, the CB density inside $RMW_{6–12}$ is higher for the ASI times than the SI cases, and the overall density for ASI cases is also more asymmetric, with a higher density in the downshear region. Neither set has a high density of CBs outside $RMW_{6–12}$. For Bill, the ASI cases have a much higher density than the SI cases inside $RMW_{6–12}$. The SI cases also have a slightly higher density outside $RMW_{6–12}$. An interesting feature of the Bill ASI composite is the large CB density near the center, in a region that is a local minimum for most of the other subgroups. A more detailed look at these cases reveals that in the ASI cases early in the life cycle of Bill (hours 36–40, which seemed to correspond to the beginning of a longer RI period), the eye had not yet formed, based on simulated radar imagery and vertical velocity (not shown). The CBs over the center were indicative of a pattern of "extreme convection" (EC) as discussed by Gray (1998). This result indicates that CBs can play an important role in the intensification of both developing hurricanes and those with already developed eyewalls.

Once again, the differences between the sets were analyzed by using rank-sum tests to compare the difference in CB counts (Tables 3 and 4). The ASI cases have an even higher density of CBs inside $RMW_{6–12}$ than do the SI cases. For Dean, there are also fewer CBs outside $RMW_{6–12}$ for the ASI cases than for SI cases, although this difference is not statistically significant for Bill. Also, the difference in counts between CBs inside and outside $RMW_{6–12}$ is statistically significantly higher for the ASI cases. These results suggest that in addition to distinguishing between intensifying and weakening portions of the life cycle of the simulated TCs, CBs may also be a sign that ASI will soon begin or is ongoing (again, at least for cases like those examined here). This point will be explored in more detail later.

### 3) FORWARD AND BACKWARD INTENSITY CHANGE

Thus far, the results mainly confirm what much recent work has shown: that CBs inside the RMW are associated with intensification, including ASI. To make full use of the high resolution of the model data used here, and answer some of the questions about the CB–intensity

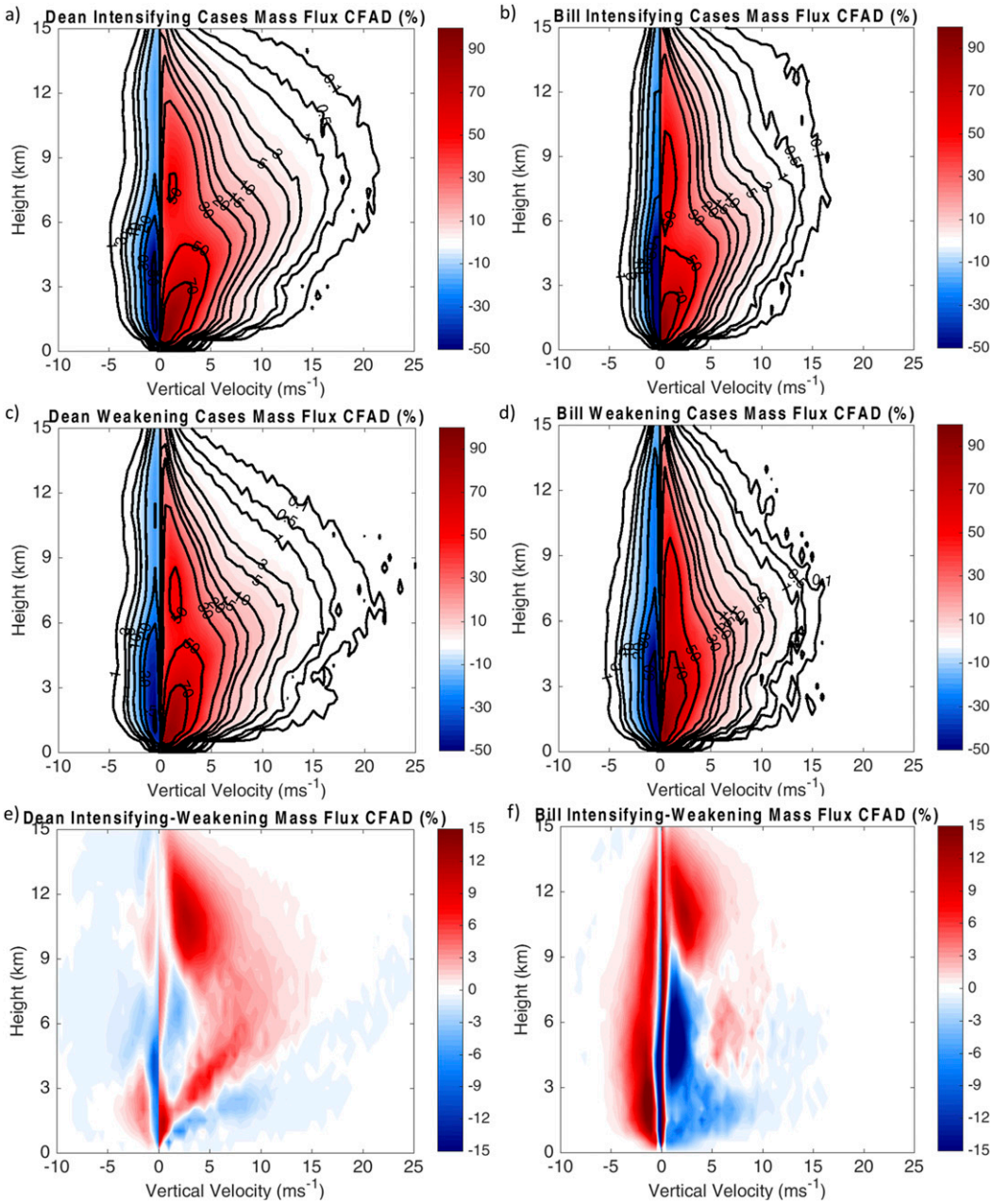


FIG. 4. (a) CFAD of normalized vertical mass flux as a function of height and vertical velocity for the cases in the Dean simulation where the storm was about to intensify in the following 3 h. (b) As in (a), but for the Bill simulation. (c) As in (a), but for cases where Dean was about to weaken in the following 3 h. (d) As in (c), but for the Bill simulation. (e) The difference in intensifying and weakening CFADs for the Dean simulation. (f) As in (e), but for the Bill simulation.

change relationship, we further separate the simulations based not only on forward 3-h intensity change but also based on backward 3-h intensity change. This separation allows for an assessment of the impact of intensity change that is already ongoing (i.e., to see if intensity change typically precedes CB development or vice versa). Thus, there are now four groups for each simulation: intensification followed by additional intensification (II), intensification followed by a weakening/steady-state period (IW), a weakening/steady period followed by intensification (WI), and a weakening/steady period followed by additional weakening (WW).

Figures 6 and 7 show CB densities for each of these four groups for each simulation. Once again, the counts

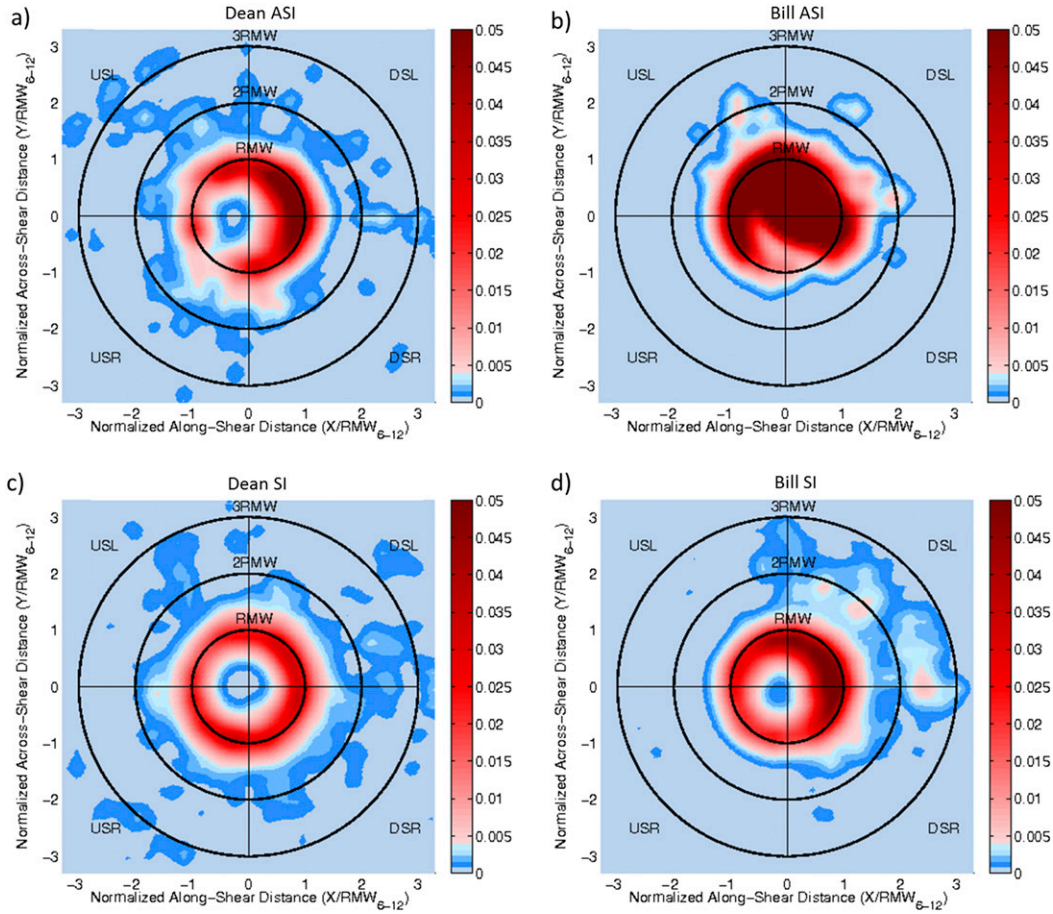


FIG. 5. (a) Density of CBs in the Dean simulation prior to periods of abrupt short-term intensification. (b) As in (a), but for the Bill simulation. (c) Density of convective bursts in the Dean simulation prior to intensifying time periods below the abrupt short-term intensification threshold. (d) As in (c), but for the Bill simulation. The CB densities are again normalized by the sample size of each group for comparison.

are normalized for comparison. For Dean, the II cases have the highest and most symmetric distribution of CBs inside $RMW_{6–12}$. This symmetry is generally consistent with the findings of Zagrodnik and Jiang (2014). The IW cases have a similarly high density inside $RMW_{6–12}$ but also more CBs outside $RMW_{6–12}$. Interestingly, the WI cases do not have a much larger density inside $RMW_{6–12}$ than do the WW cases, and the density/symmetry is much lower than in the II cases. This result implies that CBs were most associated with intensification when the storm was already intensifying in the Dean simulation, rather than before the initiation of intensification. Thus, although CBs can be associated with and aid in intensification, they may not always initiate intensification. WW has a much higher density outside $RMW_{6–12}$ than the other groups.

TABLE 3. Comparison of CB counts (per model output time) inside and outside the RMW, as well as the difference between the counts inside and outside (per model time), for the Dean WRF simulation for times when the forward intensification was greater than or equal to 3 hPa $(3\,h)^{-1}$ and times when the forward intensification was between 0.5 and 3 hPa $(3\,h)^{-1}$. Statistical relationships between the categories are also quantified. Relationships significant at the 90% level are italicized, relationships significant at the 95% level are set in boldface, and relationships significant at the 99% level are boldface and italicized.

| | CBs inside RMW | CBs outside RMW | Difference |
|---|---|---|---|
| ASI Mean (median) | 8.8 (5) | 3.5 (2) | 5.3 (2) |
| SI Mean (median) | 6.2 (3) | 5.4 (4) | 0.7 (0) |
| Rank-sum test results ($p$ value) | **ASI** > **SI** ($p = 0.02$) | ***ASI*** < ***SI*** ($p < 0.01$) | ***ASI*** > ***SI*** ($p < 0.01$) |

TABLE 4. As in Table 3, but for the Bill simulation.

| | CBs inside RMW | CBs outside RMW | Difference |
|---|---|---|---|
| ASI Mean (median) | 33.0 (30) | 3.7 (3) | 29.3 (26) |
| SI Mean (median) | 9.8 (7) | 3.0 (2) | 6.8 (5) |
| Rank-sum test results ($p$ value) | ***ASI*** > ***SI*** ($p \leq 0.01$) | *ASI* > *SI* ($p = 0.08$) | ***ASI*** > ***SI*** ($p < 0.01$) |

For Bill, the results are qualitatively similar. The II cases have the most CBs inside the RMW. The IW cases, although still having CBs inside $RMW_{6–12}$, also have a significant number outside, especially in the downshear region. The WI cases actually have *fewer* CBs inside $RMW_{6–12}$ than do the WW cases, but once again the WW cases have by far the most CBs outside $RMW_{6–12}$, mainly concentrated in the downshear region. This difference between CBs inside and outside $RMW_{6–12}$ for the different groups further supports the importance of the radial location of CBs for regulating intensity change.

As with the other categories, the forward–backward intensity change groups were compared by calculating the means–medians of the distributions, and using a Wilcoxon rank-sum test to assess the significance of the difference in the distributions. These results are summarized in Tables 5 and 6. For both simulations, the II group has the highest median density inside $RMW_{6–12}$ and is significantly greater than WI and WW, but the difference is only marginally significant ($p = 0.08–0.09$) compared to IW. For Bill, the IW group has significantly more CBs outside $RMW_{6–12}$ than II, but this difference

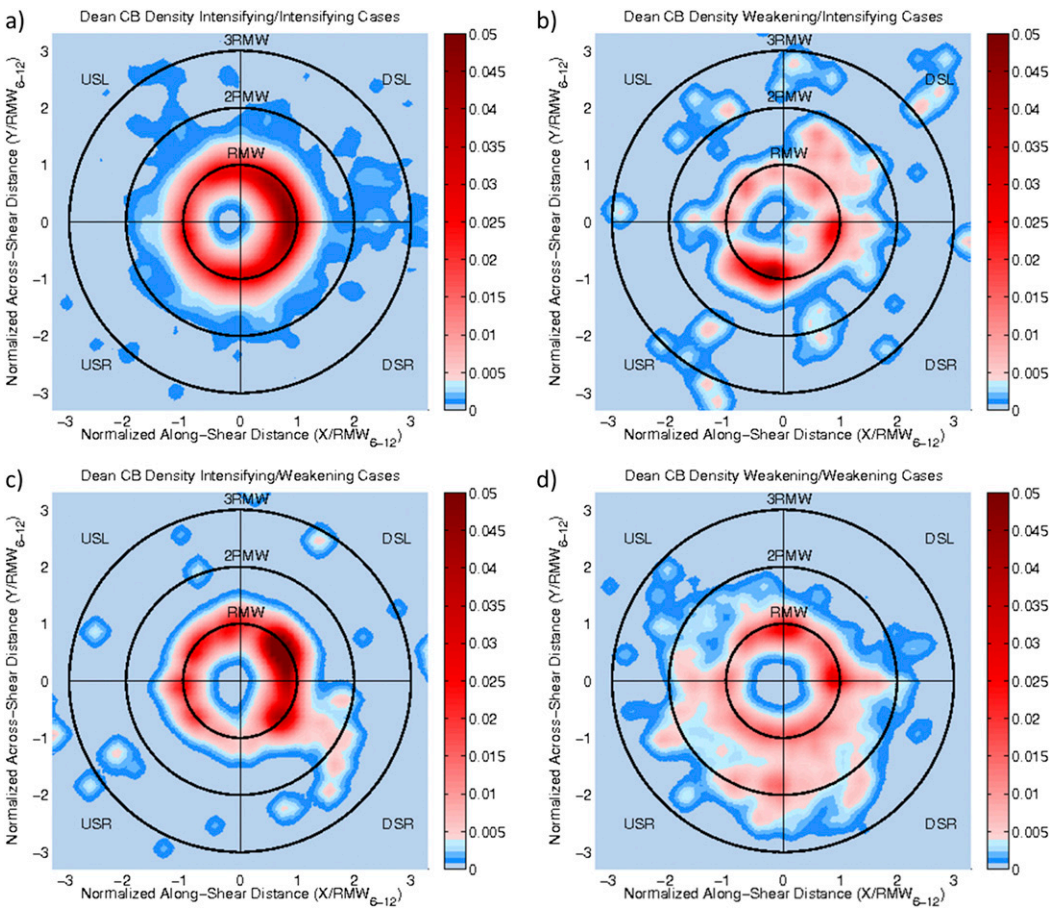


FIG. 6. Density plot of CBs in the Dean WRF run for (a) cases that had been intensifying in the previous 3 h then continued to intensify, (b) cases that had been weakening in the previous 3 h and then intensified, (c) cases that had been intensifying in the previous 3 h and then weakened, and (d) cases that had been weakening in the previous 3 h and continued to weaken. The horizontal axes are scaled by the 6–12-km RMW mean. The densities are again normalized to account for the different sample sizes in each group.

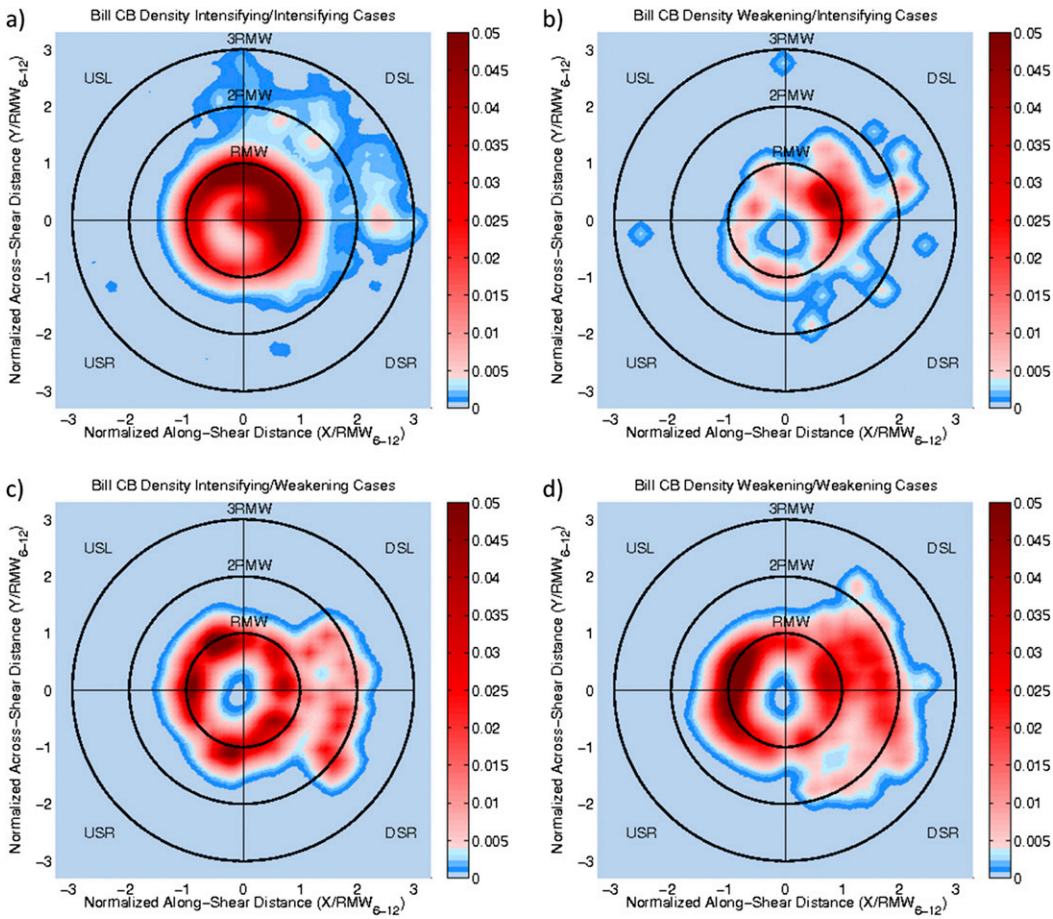


FIG. 7. As in Fig. 6, but for the Bill simulation.

is not significant in the Dean simulation. For Bill, the WW group has significantly more CBs outside $RMW_{6–12}$ than the other groups, perhaps because of the shear influence in the weakening stage. For Dean, the difference is not as pronounced, but WW does have more CBs outside $RMW_{6–12}$ than WI.

Figures 3–7 and statistical results indicate that CBs inside $RMW_{6–12}$ are clearly associated with intensification, especially when the TCs were already intensifying. Furthermore, the figures indicate that azimuthal symmetry of convection also is associated with intensification. This result is most true, though, when the storm was already intensifying. In both cases, CBs outside the RMW are an indicator of weakening. The timing and potential predictive power of CBs is explored next using lag correlations between CBs and intensity change.

### b. *Lag correlations between CBs and intensity change*

To further explore the time scale of the connection between CBs and intensity change, lag correlations between intensity and CB counts inside and outside $RMW_{6–12}$ are calculated. These lag correlations extend from −6 to +6 h, with negative (positive) times indicating intensity change leading (lagging) CBs. The results are shown in Fig. 8 for each shear-relative quadrant, as well as for the sum of all quadrants. For both cases, the CBs inside the RMW show a correlation with pressure falls, as expected. The strongest relationship with intensity change is found in the downshear quadrants for both simulations, where CBs are most concentrated. The correlation is weakest around 0 lag, and there is some future intensity change associated with CBs inside the RMW, as most of the correlations are highest at positive lead around 1–3 h. However, the correlations also indicate a relationship with CBs lagging intensity change, perhaps during long periods of ongoing intensification (which both storms experienced). The $p$ values (not shown) indicate that the relationships in all quadrants become insignificant (>0.05) past ~4-h lag in the Dean case, but are slightly stronger in the Bill case (mainly in the downshear quadrants).

TABLE 5. Comparison of mean and median CB counts (per model output time) inside and outside the RMW, as well as the difference between the counts inside and outside (per model time), for the Dean WRF simulation broken down by four intensity change categories: intensification followed by intensification, weakening followed by intensification, intensification followed by weakening, and weakening followed by weakening. Statistical relationships between the categories are also quantified. Relationships significant at the 90% level are italicized, relationships significant at the 95% level are set in boldface, and relationships significant at the 99% level are boldface and italicized.

| | CBs inside RMW | CBs outside RMW | Difference |
|---|---|---|---|
| II Mean (median) | 7.4 (4) | 5.0 (3) | 2.4 (0) |
| WI Mean (median) | 3.9 (0) | 3.4 (3) | 0.5 (−2) |
| IW Mean (median) | 5.9 (1.5) | 4.6 (3) | 1.3 (0) |
| WW Mean (median) | 3.4 (0) | 5.7 (4) | −2.3 (−2) |
| Rank-sum test results ($p$ value) | ***II*** > ***WI*** ($p < 0.01$) | II = WI ($p = 0.19$) | **II** > **WI** ($p = 0.04$) |
| | *II* > *IW* ($p = 0.08$) | II = IW ($p = 0.20$) | II = IW ($p = 0.38$) |
| | **II** > **WW** ($p < 0.01$) | II = WW ($p = 0.10$) | **II** > **WW** ($p < 0.01$) |
| | WI < IW ($p = 0.15$) | WI = IW ($p = 0.50$) | WI = IW ($p = 0.21$) |
| | WI = WW ($p = 0.30$) | **WI** < **WW** ($p = 0.03$) | *WI* > *WW* ($p = 0.06$) |
| | **IW** > **WW** ($p = 0.04$) | *IW* < *WW* ($p = 0.08$) | **IW** > **WW** ($p < 0.01$) |

However, the highest correlations are actually found for negative lag, consistent with the composite findings above, with the CB density highest in cases that were already intensifying and continuing to intensify.

Figures 8c and 8d show a slightly more complicated picture with CBs outside $RMW_{6–12}$ for both Dean and Bill. The azimuthally summed CB correlations with intensity change are weaker (especially for the Bill simulation), possibly because CBs outside $RMW_{6–12}$ can sometimes occur simultaneously with CBs inside $RMW_{6–12}$, causing competing influences on intensity change. This effect can also be seen in the fact that the DSL quadrant in Dean actually has a slightly negative relationship at positive lead (indicating CBs outside the RMW before intensification). However, most of the correlations (especially for Dean) are slightly positive, indicating that CBs outside the RMW are associated with pressure rises. However, the $p$ values (not shown) indicate that most of these relationships with CBs outside $RMW_{6–12}$ are weak and not significant at most lead times.

There is an interesting split for Bill at positive lead, with the USL quadrant showing a negative relationship (i.e., CBs outside correlated with pressure falls), with the DSL region showing a correlation between CBs outside the RMW and pressure rises (although not statistically significant). This relationship could be due to shear, with more CBs able to persist into the upshear region during times with weaker shear, leading to intensification. Also, the times with higher shear (leading to weakening) could have more CB generation in the downshear-right region, further complicating the correlation. As mentioned above though, the relationships are generally weaker, and future work is needed to examine the importance of other factors such as the specific radial locations of CBs outside the RMW. The next section will attempt to show some of these relationships and competing effects in detail by looking at individual periods in each simulation.

### c. *Analysis of CBs and intensity change during individual time periods*

To explore the relationship between CBs and intensity change in more detail, individual time periods in the life cycle of each simulated TC are examined. These include periods at the beginning of intensification/ASI as well as periods when the intensification is ending and

TABLE 6. As in Table 5, but for the Bill simulation.

| | CBs inside RMW | CBs outside RMW | Difference |
|---|---|---|---|
| II Mean (median) | 13.7 (11) | 3.3 (2) | 10.4 (8) |
| WI Mean (median) | 3.3 (2) | 2.2 (1) | 1.1 (0) |
| IW Mean (median) | 8.2 (8) | 5.3 (5.5) | 2.9 (3.5) |
| WW Mean (median) | 8.7 (7) | 8.1 (7) | 0.6 (0) |
| Rank-sum test results ($p$ value) | ***II*** > ***WI*** ($p < 0.01$) | **II** > **WI** ($p = 0.05$) | ***II*** > ***WI*** ($p < 0.01$) |
| | *II* > *IW* ($p = 0.09$) | ***II*** < ***IW*** ($p < 0.01$) | ***II*** > ***IW*** ($p = 0.01$) |
| | ***II*** > ***WW*** ($p < 0.01$) | ***II*** < ***WW*** ($p < 0.01$) | ***II*** > ***WW*** ($p < 0.01$) |
| | ***WI*** < ***IW*** ($p < 0.01$) | ***WI*** < ***IW*** ($p < 0.01$) | WI = IW ($p = 0.15$) |
| | ***WI*** < ***WW*** ($p < 0.01$) | ***WI*** < ***WW*** ($p < 0.01$) | WI = WW ($p = 0.32$) |
| | IW = WW ($p = 0.40$) | *IW* < *WW* ($p = 0.06$) | IW = WW ($p < 0.12$) |

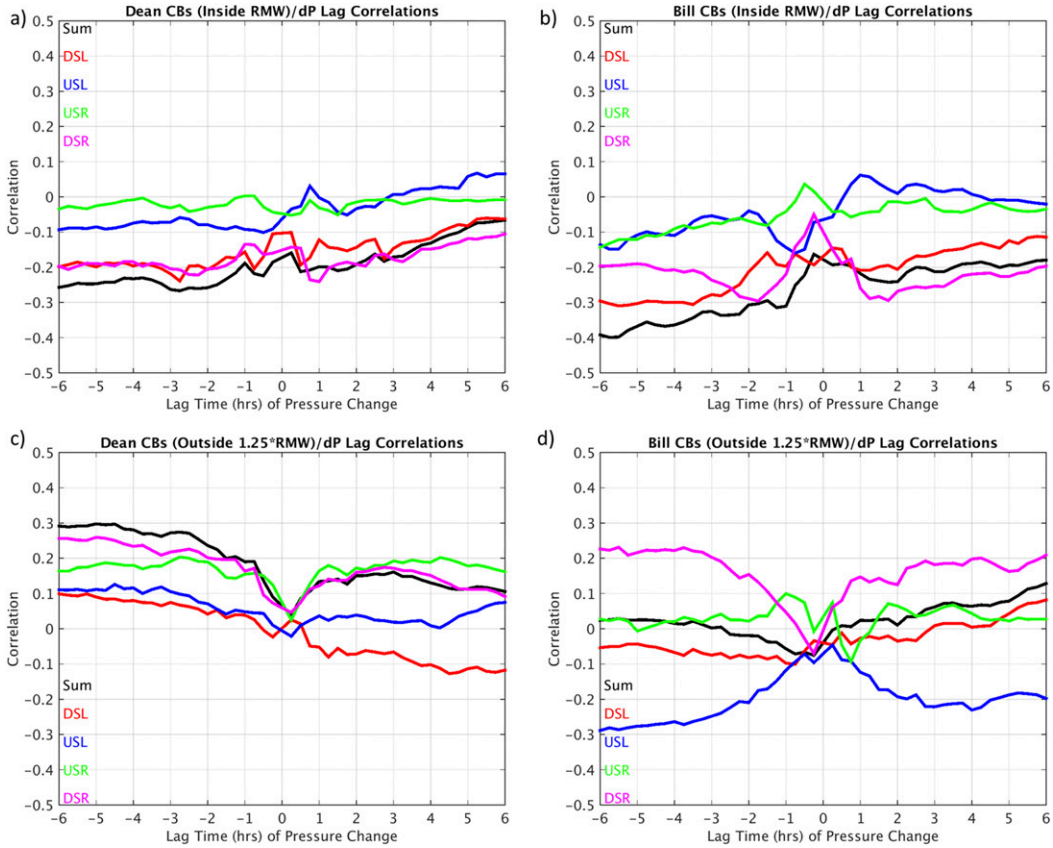


FIG. 8. (a) Lag correlations for the Dean simulation between CB counts inside the RMW (in each shear-relative quadrant and summed together) and intensity change. Negative times indicate intensity change leading CBs and positive times indicate CBs leading intensity change. (b) As in (a), but for the Bill simulation. (c) As in (a), but with CBs outside the RMW instead of inside. (d) As in (c), but for the Bill simulation.

weakening is beginning. This analysis will allow for study of the impact of CBs on different aspects of intensity change. In addition, the roles of environmental factors versus CBs in driving intensity change are assessed.

### 1) DEAN SIMULATION HOURS 19–27

The first time period examined covers hours 19–27 of the Dean simulation. As can be seen in Fig. 1, this was during an early period of intensification. Figure 9 shows the time series of CBs and intensity change during this time period. Figure 9 also shows the temperature anomaly in the center of the TC based on two definitions: 1) the temperature difference between the center of the storm and the azimuthal mean temperature at $4 \times \mathrm{RMW}_3$ averaged over the entire simulation and 2) the temperature difference between the center and the Dunion mean tropical sounding (Dunion and Marron 2008). The environment-relative warm core in Fig. 9b shows a maximum in the low to midtroposphere, similar to that in Stern and Nolan (2012). The second method, which removes any possible contamination due to the warm core of the storm itself, shows more of an upper-level maximum. However, the trends in the magnitude of the warm core are similar using both methods. As can be seen, the intensification is initially slow. A small spike in CB activity occurs around hour 20, followed by an increase in warm core magnitude. This increase does not appear to persist, but around hour 23, a period of ASI begins just after (or concurrently with) a major spike in CB activity inside the RMW. During this time period, the magnitude and depth of the warm core is seen to increase markedly, indicating a relatively direct response of the vortex to CB activity. There is a 2–3-h lag between the peak in CB activity and the maximum deepening of the warm core, consistent with the lag correlations (on the positive side) discussed above. However, the intensification also seemed to begin around the same time as the CB spike, consistent with the findings of McFarquhar et al. (2012) and Zagrodnik and Jiang (2014), indicating that other processes (such as

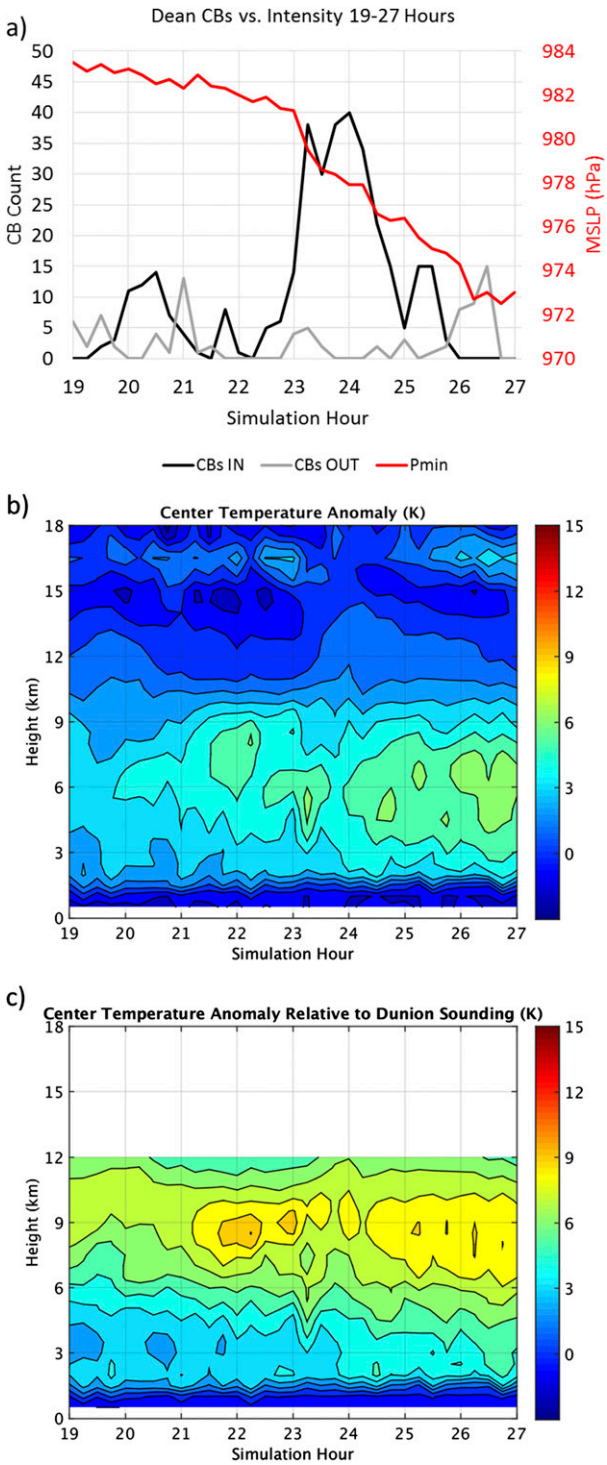


FIG. 9. (a) Time series of CBs inside and outside the RMW, as well as minimum pressure, from hours 19.0–27.0 of the Dean simulation. (b) Time evolution of the center temperature anomaly relative to the environmental temperature from hours 19.0 to 27.0 of the Dean simulation. (c) As in (b), but relative to the Dunion mean tropical sounding instead of the local environment.

contributions from weaker updrafts) may also be playing a role during this time period.

### 2) DEAN SIMULATION HOURS 115–125

As Fig. 1 shows, the period from hours 115 to 125 of the Dean simulation marked the end of the major intensification and the beginning of a weakening period. Figure 10 shows the time series of CBs inside and outside $RMW_{6–12}$, the intensity, and the warm core structure during this time period. Early on, as the storm is intensifying, there are large numbers of CBs inside $RMW_{6–12}$. However, after a spike at the end of the intensification period (perhaps associated with the ongoing intensification) these numbers drop off with time to near zero after hour 122. Around the same time, the CB count outside the RMW begins to increase. The depth and magnitude of the warm core decreases slightly at upper levels while remaining approximately constant at midlevels, and the weakening period commences. This period of enhanced CBs outside the RMW as weakening begins is consistent with the composite results, with the IW composite showing more CBs outside $RMW_{6–12}$ than II.

Next, some possible reasons for this increase in outer-core CBs and weakening are explored. There was an increase in shear, but only to 10–15 kt (where $1\,\mathrm{kt} = 0.5144\,\mathrm{m\,s^{-1}}$), and the outflow was not significantly affected (not shown). Dry air was not a major issue for the simulated TC, so it appears that internal dynamics associated with secondary eyewall formation (SEF) may have played a role (e.g., Willoughby et al. 1982; Willoughby 1990; Kossin and Sitkowski 2009). This process is illustrated in Fig. 11, which shows the convective structure at hours 115.0, 123.0, and 125.0, as approximated by the 6–15-km ice (cloud ice, snow, and graupel) mixing ratio. These data are compared with an observed 85-GHz microwave image at approximately 1200 UTC 19 August, ~12–18 h earlier than the simulation times (around the time the actual TC began to weaken). The model ice mixing ratio is not intended to directly simulate the microwave image, but rather both are intended to approximate the convective and precipitation structures. The structures are similar, with an inner eyewall plus a developing, prominent band or secondary eyewall that grows with time. There is some time lag between the model and observations, as there was in the intensity evolution, but just as the observed storm was in a weakening trend during this time period, it appears the development of the secondary eyewall (with CBs found outside the RMW) and associated decay of the inner eyewall (as seen in Fig. 10c) were largely responsible for the weakening during this period.

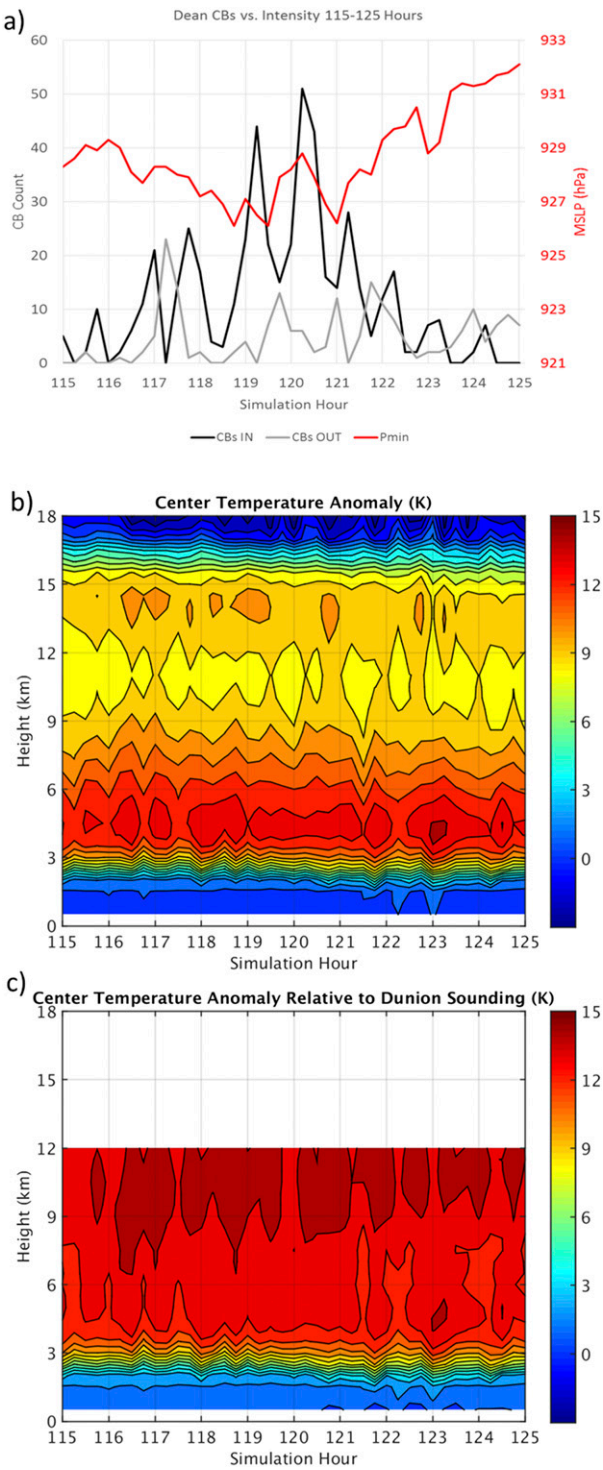


FIG. 10. As in Fig. 9, but for hours 115.0–125.0 of the Dean simulation.

### 3) DEAN SIMULATION HOURS 134–144

The next period covers the end of the weakening period and beginning of the reintensification of Dean at the end of the simulation, as seen in Fig. 1. The intensity evolution, CB counts, and warm core structure during these 10 h are shown in Fig. 12. Early in this period, there was little CB activity. During this first ~3 h, the warm core did not change much, and the intensity was mostly steady (with gradual intensification perhaps beginning). However, around hour 137.0 the CB counts inside the RMW increased, and the warm core (both mid- and upper levels) began to strengthen and deepen. The storm intensified very rapidly starting around hour 137.5, with the pressure falling approximately 11 hPa in 6 h. In this case, there was a slight time lag, with the ASI beginning about an hour after the CBs increased and continuing in conjunction with increased CB activity. This result indicates that, as the composites showed, most CBs are found when the storm is already intensifying, but CBs can also mark the start of a more pronounced intensification period, as seen here.

### 4) BILL SIMULATION HOURS 54–64

The first period analyzed in Bill is from hours 54 to 64. As Fig. 1b shows, intensification onset occurred during this period. Figure 13 shows the intensity, CBs inside and outside the RMW, and warm core structure from hours 54 to 64. This is another case where CB development and intensity change are connected. The intensity was slowly increasing or steady for the first 5 h, but around hour 59, the warm core magnitude and depth increases and the period of intensification begins. In this case, the spike in CB activity occurs prior to the intensification beginning, with CBs increasing from hours 56 to 58. In this case, there is a lag of about 2–3 h between CBs inside the RMW and the beginning of deepening. Notice that the CB counts decrease around hours 59–60 and 61–61.5, with brief lulls in intensification following. However, as the spikes in CB activity occur, intensification resumes almost immediately after, with the depth and strength of the warm anomaly increasing as an upper-level warm maximum developed.

### 5) BILL SIMULATION HOURS 88–100

The final time period analyzed covers hours 88.0–100.0 of the Bill simulation, and includes the end of the intensification and beginning of weakening of Bill. Figure 14 shows the intensity evolution, CBs, and warm core during this time period. Early in the period, there is some CB activity inside the RMW, and the TC is intensifying slightly. Around hours 92–93, the CB counts decrease significantly, and the weakening period commences. The midlevel warm anomalies remain relatively steady, but the upper-level warm anomalies decay slightly. Interestingly, CB counts both inside and outside the RMW increase starting around hour 95, but the TC

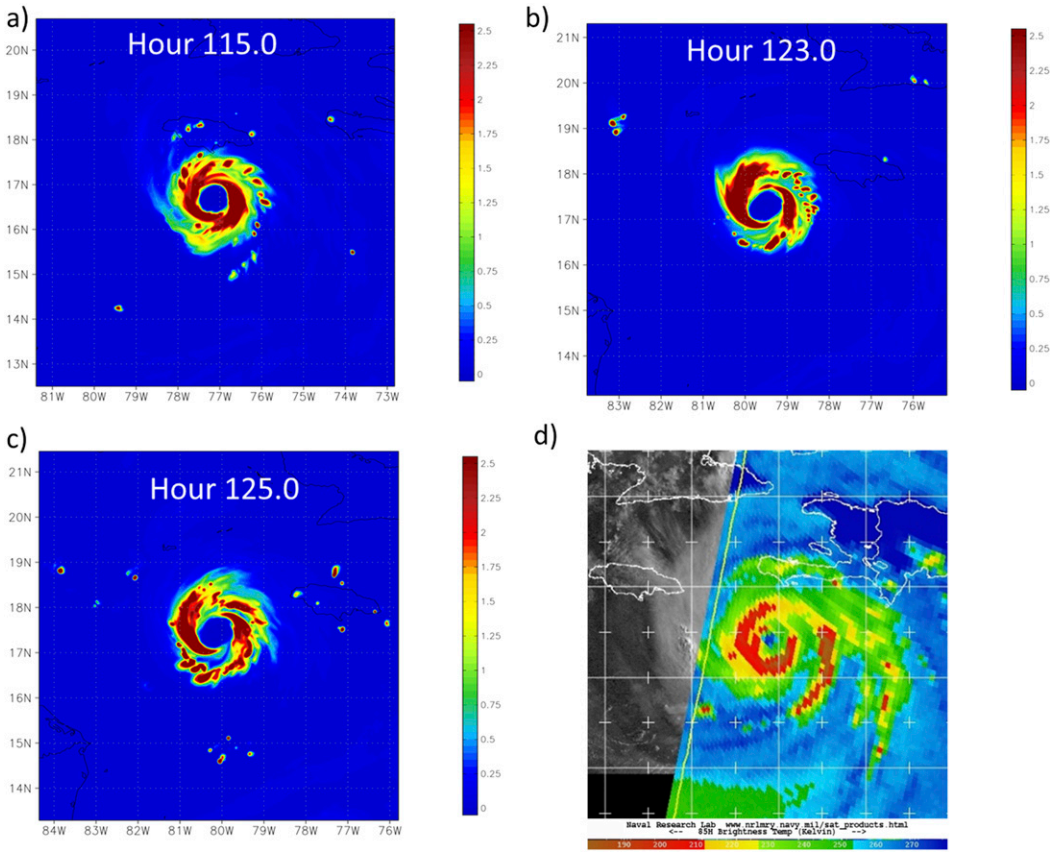


FIG. 11. (a) Simulated 6–15-km mean ice (cloud ice, snow, graupel) mixing ratio (g kg$^{-1}$) for hour 115.0 (1900 UTC 19 Aug 2007) of the Dean simulation. (b) As in (a), but for hour 123.0 (0300 UTC 20 Aug 2007) of the Dean simulation. (c) As in (a), but for hour 125.0 (0500 UTC 20 Aug 2007) of the Dean simulation. (d) Observed 85-GHz microwave image of Hurricane Dean at 1117 UTC 19 Aug 2007. [Image provided by the Naval Research Laboratory (NRL 2015).]

continues to weaken. Figure 15 shows the ice mixing ratio during this period and observed microwave imagery from approximately the same time. Note the decrease in eyewall symmetry during the period, with the eyewall becoming open on the southern side (similar to the asymmetry seen in the observations, although the model eye is too large). It appears that the large-scale environment (examined next) perhaps led to weakening and (simultaneous) CB development outside the RMW.

Figures 16a–c show the 5–10-km mean relative humidity at hours 88, 96, and 100. Notice that initially, the moisture is relatively symmetric around the TC. However, with time, the southwest side begins to dry out, as a result of advection from the environment and/or subsidence from a shear-induced wavenumber-1 asymmetry due to the increase in deep-layer southwesterly vertical shear during this time period (as seen in Fig. 1 of Part I). The shear increased from ~11 kt at hour 88 to 20 kt by hour 96. Early in the period, with weak shear, the outflow aloft was unrestricted on all sides. The increasing shear restricted outflow as time went on, as seen in Figs. 16d and 16f. This increasing shear was likely at least partially responsible for some of the weakening and reduction of the upper-level warm anomalies (e.g., Frank and Ritchie 2001) despite forcing CB development. This case may illustrate how, in some cases, the external forcing from the TC environment can overwhelm the internal forcing and cause weakening even when convective activity is occurring in the eyewall region.

## 4. Discussion

This analysis further showed the nature of the TC response to CBs, extending the results from Part I. Further, it provided an opportunity to compare CBs and the associated intensity changes in both low- and high-shear environments. Inner-core processes were important in both simulations, with environmental interaction also playing a large role particularly in the Bill simulation.

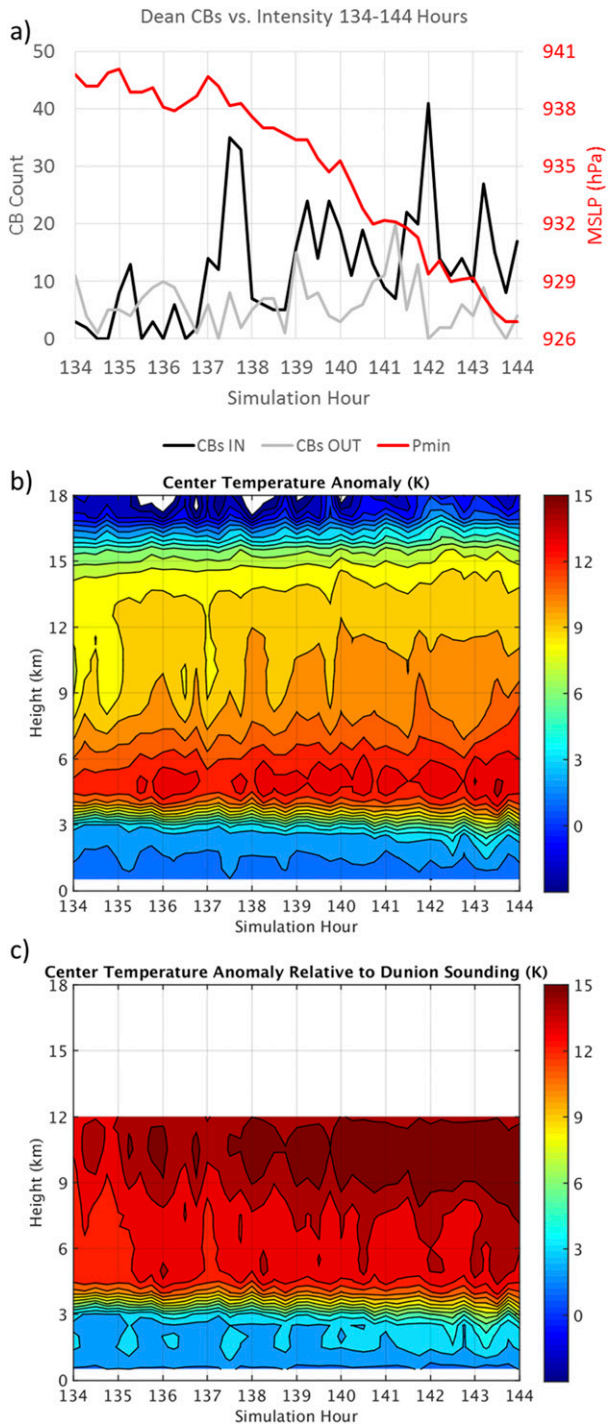


FIG. 12. As in Fig. 9, but for hours 134.0–144.0 of the Dean simulation.

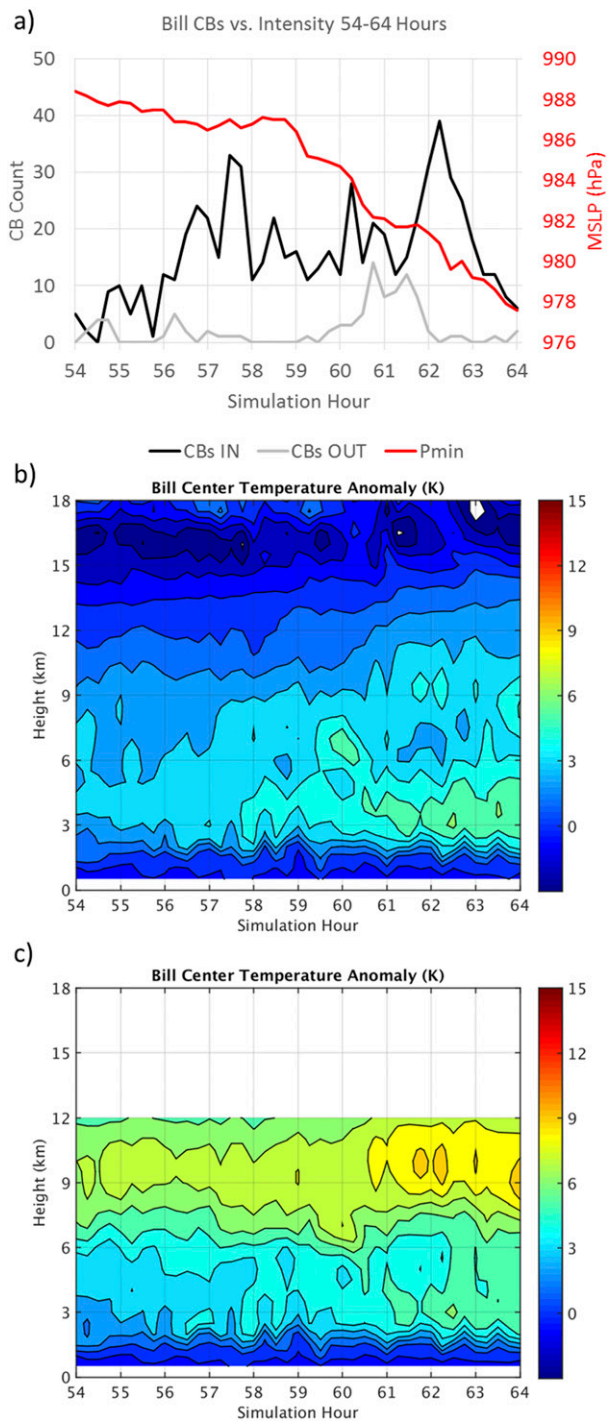


FIG. 13. As in Fig. 9, but for hours 54.0–64.0 of the Bill simulation.

The separation by forward intensity change confirmed a relationship between CB development and intensity change. For the Dean simulation, there is a higher density of CBs inside $RMW_{6–12}$ for time periods where the TC is about to intensify than for times when it is about to weaken, and the weakening/steady times have a slightly higher density outside $RMW_{6–12}$. For Bill, the distribution of the CBs is similar, and the difference outside the RMW is even more pronounced, especially in the downshear region of the TC. This result is likely due to the higher shear encountered by Bill, especially at the end of its life

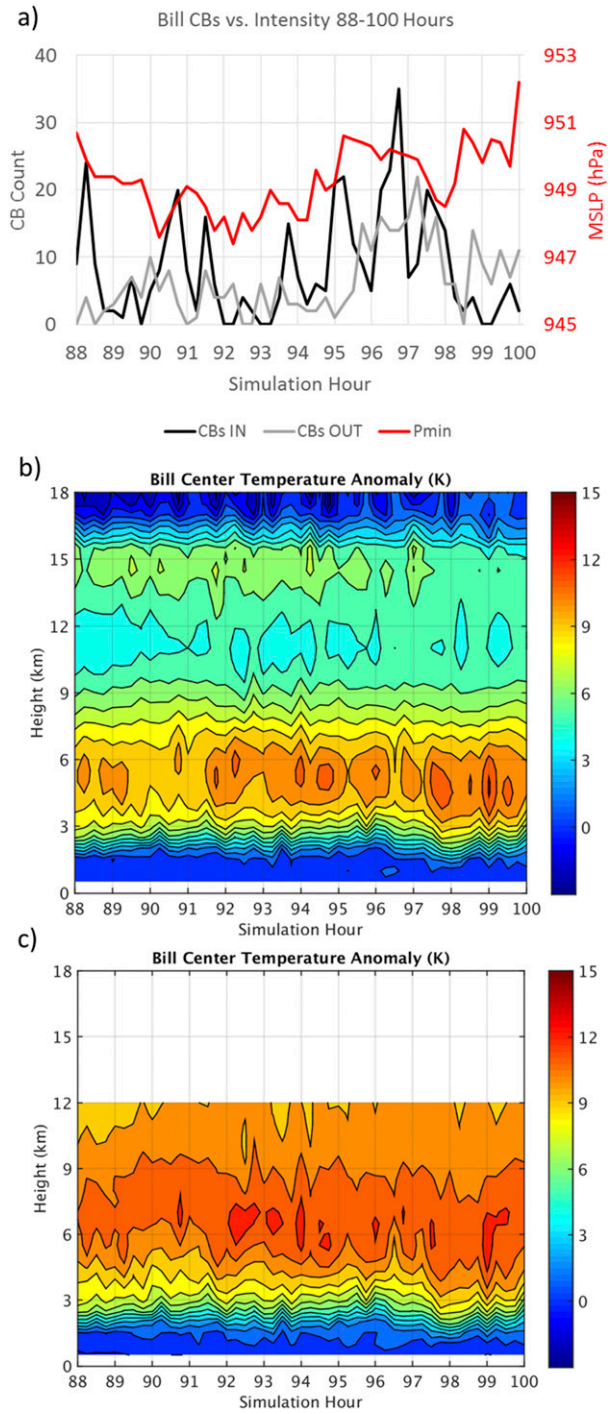


FIG. 14. As in Fig. 9, but for hours 88.0–100.0 of the Bill simulation.

cycle (discussed in Part I), which induced a pronounced wavenumber-1 asymmetry in vertical motion. This difference in CBs outside and inside $RMW_{6–12}$ for intensifying and weakening/steady TCs is consistent with the findings of Rogers et al. (2013), and the largest differences found at higher percentiles of vertical velocity also indicate that the CBs in these simulations provide a clear indication of impending or ongoing intensity changes, similar to what was found in that observational study. This difference also makes sense from a theoretical perspective. When the convective bursts occur inside the RMW, the heating due to convection occurs in the high inertial stability region of the TC and can lead to pressure falls in the inner-core region and TC intensification. When the CBs occur farther outward, the heating is not as efficient and does not result in significant pressure falls in the inner core. This difference is described in studies such as those by Hack and Schubert (1986) and Vigh and Schubert (2009). Recent work by Smith and Montgomery (2016) takes a different perspective, instead arguing that TC intensification occurs because of the spinup of the tangential winds by the import of angular momentum in the PBL. The warm core deepening, then, is a response rather than a cause of intensification in this perspective. CBs could act in a kinematic sense to strengthen the TC through increased inflow, rather than directly impacting the TC thermodynamics. Regardless of which role is dominant, inflow and convergence inside the RMW are important for intensification. Future work could explore these different mechanisms directly in these or other simulations.

The vertical mass flux distributions helped in developing a better understanding of the contributions of CBs to intensity change within the context of the total vertical mass flux and vertical velocity. Consistent with Rogers (2010) and Rogers et al. (2013), the bulk of the updraft mass flux was accomplished by weak updrafts (0–$2\,\mathrm{m\,s^{-1}}$). However, in contrast to the numerical study of Rogers (2010), the greatest differences in updraft mass flux between intensifying and weakening cases were found at upper levels. Although the largest differences between weakening and intensifying cases were found in the weak updrafts, there was also a notable increase in mass flux from extreme updrafts (above $\sim 5\,\mathrm{m\,s^{-1}}$) for the intensifying cases in both simulations, providing support for further examination of the role of CBs.

Because of the high temporal resolution, the simulations (and CB distributions) could be further stratified by the rate of TC intensification. The intensifying times were separated into periods of abrupt ASI and SI, and the CB distributions were examined for each of these groups. The density/counts of CBs were higher inside $RMW_{6–12}$ prior to ASI than prior to SI. The formation of convective towers prior to rapid intensity change has been observed in some recent studies (both numerical and observational), including those by Monette et al. (2012) using infrared satellite data, Chen and Zhang (2013) using a simulation of Hurricane Wilma (2005), and Stevenson et al. (2014) using lightning data in Hurricane Earl (2010). These findings are echoed in the

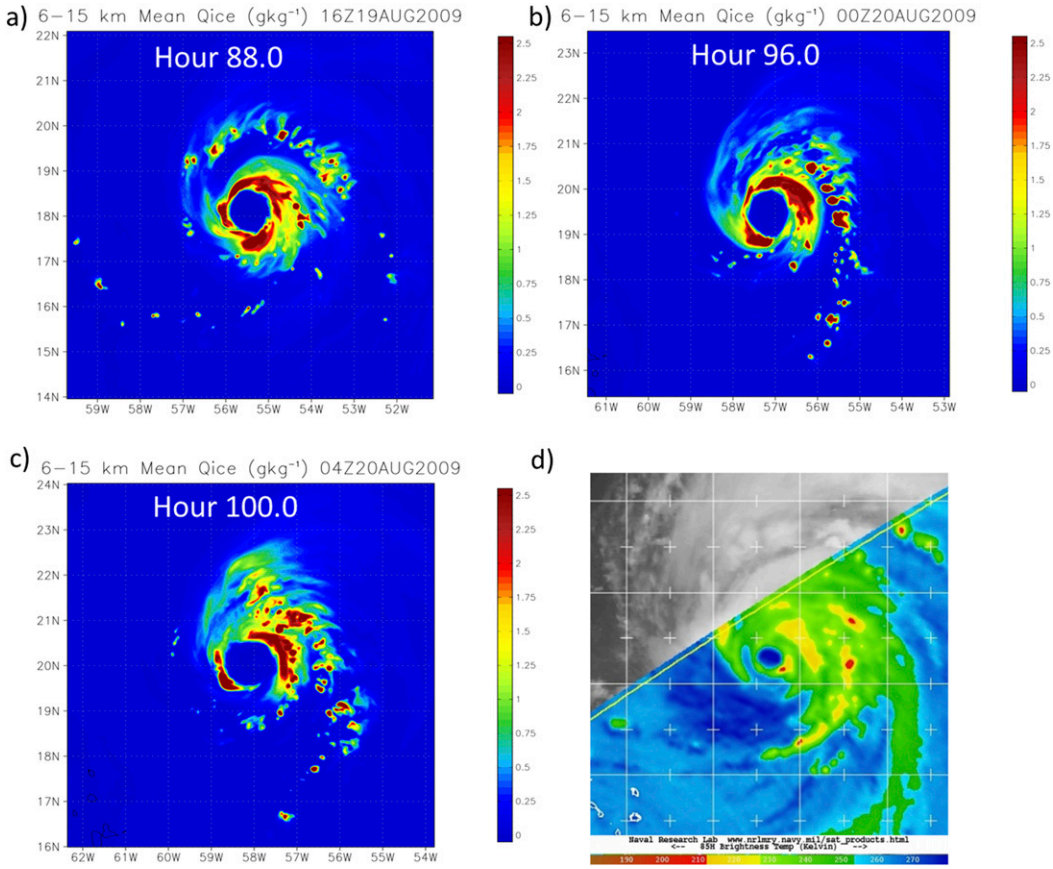


FIG. 15. (a) Simulated 6–15-km mean ice (cloud ice, snow, graupel) mixing ratio ($g\,kg^{-1}$) for hour 88.0 (1600 UTC 19 Aug 2009) of the Bill simulation. (b) As in (a), but for hour 96.0 (0000 UTC 20 Aug 2009) of the Bill simulation. (c) As in (a), but for hour 100.0 (0400 UTC 20 Aug 2009) of the Bill simulation. (d) Observed 85-GHz microwave image of Hurricane Bill at 0208 UTC 20 Aug 2009. [Image provided by the Naval Research Laboratory (NRL 2015).]

results for this analysis, showing that CBs are associated with ASI, both before the eye develops and after. This latter point is the reason for the high density of CBs observed very near the center in the composite for Bill, with CBs helping to spin up the inner-core region early in the simulation. The process seen early in the Bill simulation is qualitatively similar to the area of EC in developing TCs discussed by Gray (1998). These findings imply that CBs precede ASI, as the definition was based on forward intensity change. This result is qualitatively consistent with the idealized studies of Möller and Montgomery (1999) and Enagonio and Montgomery (2001), in which convective asymmetry was found to lead to short-term intensification. Persistent and periodic "pulsing" of these asymmetries (as seen in the CBs in the current study) was found to lead to sustained intensification. Here, the CBs inside the RMW similarly appear to be associated with short-term changes in intensity, and also to contribute to longer periods of intensification during some time periods (but not in others). It should also be noted that CBs are not the sole process responsible for intensification, but may also occur as a response to other processing favoring ASI, such as a general increase in the vertical mass flux or the import of angular momentum in the PBL. In addition, the exact time scale or lag of the response is not clear from these composites. Thus, there was a need for further exploration of the intensity evolution and its connection to CBs.

The stratification by future *and* prior intensity changes provided a unique opportunity to make use of the high temporal resolution of the model data, as most previous studies had only considered the forward intensity change. Some key conclusions can be drawn. The tendency for greater CB activity inside $RMW_{6–12}$ for intensifying times and CB activity outside $RMW_{6–12}$ for weakening times is still seen. However, these differences are most pronounced for continuous intensity change (II), in other words, intensification occurring both before and after the CB activity. The transitioning (WI and IW) cases did not show as clear of a signal, and some

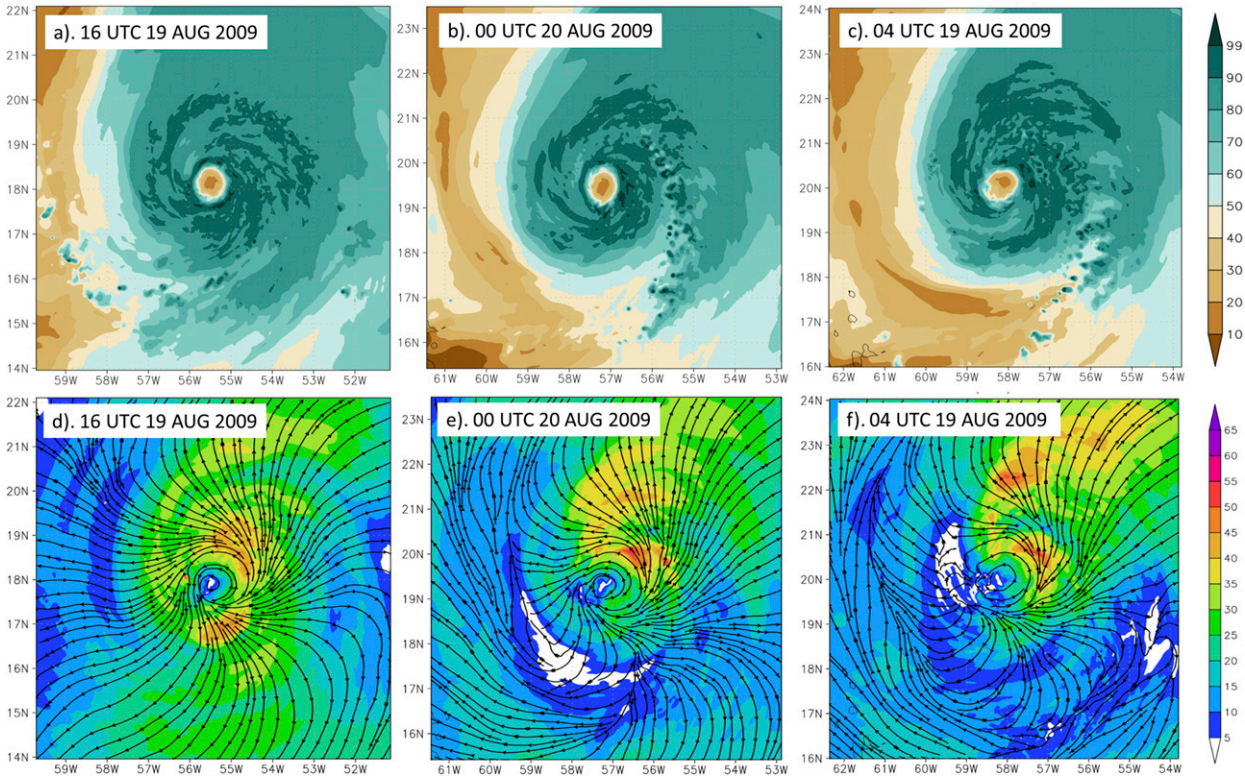


FIG. 16. (a) Simulated 5–10-km mean relative humidity for hour 88.0 (1600 UTC 19 Aug 2009) of the Bill simulation. (b) As in (a), but for hour 96.0 (0000 UTC 20 Aug 2009) of the Bill simulation. (c) As in (a), but for hour 100.0 (0400 UTC 20 Aug 2009) of the Bill simulation. (d) Simulated 15-km wind speed (kt) and streamlines for hour 88.0 (1600 UTC 19 Aug 2009) of the Bill simulation. (e) As in (d), but for hour 96.0 (0000 UTC 20 Aug 2009) of the Bill simulation. (f) As in (d), but for hour 100.0 (0400 UTC 20 Aug 2009) of the Bill simulation.

results were actually opposite of those expected (such as the WW cases for Bill actually having higher CB density inside the RMW despite also having higher density outside $RMW_{6–12}$ than II, WI, and IW). Sometimes, a storm may begin to intensify before inner-core CB activity picks up (e.g., Cecil et al. 2010; Zagrodnik and Jiang 2014), and storms may also weaken before significant CB activity develops outside the RMW (e.g., potentially because of environmental interaction). Nevertheless, the results do indicate that CB development can be useful for the prediction of intensity changes, particularly when combined with information about storm trends. This finding is consistent with the results of Zhuge et al. (2015), who found that RI predictions based on hot towers had increased skill when coupled with information about the prior intensity change as well as environmental factors related to intensity change. Thus, an intensifying storm with significant eyewall CB activity is likely to continue intensifying. Also, a storm that has been weakening or is steady state will likely not begin to intensify if it has significant convective activity outside the eyewall.

This connection between CBs and future and/or ongoing intensity change was further explored by analyzing the lag correlations between CBs and intensity changes. The results from this analysis further highlighted the idea of CBs being a predictor of intensity change on short-term time scales, as well as the importance of the connection to prior intensity change. The lag correlations between CBs and future intensity change were most significant from about 0 to 3 h. Interestingly, the correlations were similar or even slightly higher for intensity change leading CB development, again showing the importance of ongoing intensity change. The relationships were strongest with CBs in the downshear quadrants, where the highest CB counts were typically found. Also, the relationships with CBs outside the RMW were generally weaker, although these were broadly associated with future weakening (and weakening also led CBs outside the RMW in some cases, particularly for Dean).

The analysis of CB development and intensity change in individual time periods of each simulation provides further evidence for the statistical and composite results

related to intensity change, and also highlights the physical response of the TC warm core to CB development. The warm anomaly in the core grows in magnitude and depth as CBs develop inside the RMW, as was seen to occur in Hurricane Dennis (2005) by the observations of Guimond et al. (2010). This increase in warm core strength coincides with the pressure falls observed in several of the periods. In the same way, the warm anomaly weakens as the inner-core CBs decrease in coverage and intensity. For Dean, this weakening mainly occurs as a result of the development of a partial secondary eyewall (not truly concentric, but somewhat bandlike in its structure). For Bill, the weakening appears to be mostly driven by external factors including increasing southwesterly shear. The greater degree of environmental interaction in Bill was seen in multiple structural features, including this weakening as well as the tendency for a wavenumber-1 asymmetry in CBs because of shear (seen in Part I). For both TCs, the simulated structure is relatively consistent with the observed TCs (although with a time lag for Dean), including the secondary eyewall and interaction with shear, providing further evidence that the modeled processes are physically realistic.

## 5. Conclusions and future work

The results presented herein indicate that extreme updrafts played a large role in regulating the intensity change of the two simulated TCs. CBs inside the local $RMW_{6–12}$ are associated with intensification and ASI, both before the eye develops and after. This signal is most pronounced when the TC has already been intensifying, indicating that CBs are perhaps most prominent as a sign of ongoing intensification. CBs outside the RMW tend to be associated with weakening periods. In connection with prior work on this topic, this study suggests that although CBs may not be the only factor linked to intensity change, they can be used as a combination of a diagnostic and predictive tool. Further, the typical time scale of the intensity change response to CBs is found to be the intensity change lagging the CBs by ~0–3 h. As some of the cases in the Bill simulation indicated, large-scale environmental factors sometimes can overwhelm the intensity change as a result of CB development, but in many cases, especially with less environmental interaction, CBs are an important part of intensity change.

Future work could dig deeper into the details of the intensity response to CBs in different times of the storm's life cycle. Since the results here indicate that intensification follows CB development in the eyewall, but that this signature is especially pronounced when the TC was already intensifying, it might be useful to investigate whether other convective or precipitation structures (such as stratiform precipitation) might also have some predictive power in certain cases, and may complement the effects of the CBs (and other, large-scale factors such as SST and shear). It would be useful to examine the sensitivity of the results to the resolution of the model simulations. For example, it would be useful to see how the distributions of vertical velocity and intensity change are affected by simulating CBs at a very fine scale such as 250-m resolution, as Bryan et al. (2003) suggest that such resolution is necessary to more correctly simulate deep moist convection. This study also focused on the most extreme updrafts due to the differences in distributions that were observed between intensifying and weakening/steady cases. However, examining the impact of weaker updrafts would be an interesting extension of this work, based on the differences seen in the mass flux CFADs. A potential operational application of this research would be to develop a method that incorporates satellite- and/or radar-derived convective structures with kinematic information (such as the RMW) from scatterometer or radar data to evaluate the distribution of CBs in real time and to predict short-term intensity evolution based on this distribution. Such studies would further confirm the importance of small-scale extreme updrafts in the development and evolution of TCs.

*Acknowledgments.* The authors thank the staff of the FSU Research Computing Center for their assistance with troubleshooting the simulations. The comments of three anonymous reviewers led to significant improvements on an earlier version of the manuscript. ATH was supported by the FSU Legacy Fellowship.

REFERENCES

Black, M. L., J. F. Gamache, F. D. Marks Jr., C. E. Samsury, and H. E. Willoughby, 2002: Eastern Pacific Hurricanes Jimena of 1991 and Olivia of 1994: The effect of vertical shear on structure and intensity. *Mon. Wea. Rev.*, **130**, 2291–2312, doi:10.1175/1520-0493(2002)130<2291:EPHJOA>2.0.CO;2.

Braun, S. A., and L. Wu, 2007: A numerical study of Hurricane Erin (2001). Part II: Shear and the organization of eyewall vertical motion. *Mon. Wea. Rev.*, **135**, 1179–1194, doi:10.1175/MWR3336.1.

Bryan, G. H., J. C. Wyngaard, and J. M. Fritsch, 2003: Resolution requirements for the simulation of deep moist convection. *Mon. Wea. Rev.*, **131**, 2394–2416, doi:10.1175/1520-0493(2003)131<2394:RRFTSO>2.0.CO;2.

Cecil, D. J., K. R. Quinlan, and D. M. Mach, 2010: Intense convection observed by NASA ER-2 in Hurricane Emily (2005). *Mon. Wea. Rev.*, **138**, 765–780, doi:10.1175/2009MWR3063.1.

Chen, H., and D. Zhang, 2013: On the rapid intensification of Hurricane Wilma (2005). Part II: Convective bursts and the

upper-level warm core. *J. Atmos. Sci.*, **70**, 146–162, doi:10.1175/JAS-D-12-062.1.

——, and S. G. Gopalakrishnan, 2015: A study on the asymmetric rapid intensification of Hurricane Earl (2010) using the HWRF system. *J. Atmos. Sci.*, **72**, 531–550, doi:10.1175/JAS-D-14-0097.1.

Corbosiero, K. L., and J. Molinari, 2002: The effects of vertical wind shear on the distribution of convection in tropical cyclones. *Mon. Wea. Rev.*, **130**, 2110–2123, doi:10.1175/1520-0493(2002)130<2110:TEOVWS>2.0.CO;2.

DeHart, J. C., R. A. Houze Jr., and R. F. Rogers, 2014: Quadrant distribution of tropical cyclone inner-core kinematics in relation to environmental shear. *J. Atmos. Sci.*, **71**, 2713–2732, doi:10.1175/JAS-D-13-0298.1.

DeMaria, M., R. T. DeMaria, J. A. Knaff, and D. Molenar, 2012: Tropical cyclone lightning and rapid intensity change. *Mon. Wea. Rev.*, **140**, 1828–1842, doi:10.1175/MWR-D-11-00236.1.

Dunion, J. P., and C. S. Marron, 2008: A reexamination of the Jordan mean tropical sounding based on awareness of the Saharan air layer: Results from 2002. *J. Climate*, **21**, 5242–5253, doi:10.1175/2008JCLI1868.1.

——, C. D. Thorncroft, and C. S. Velden, 2014: The tropical cyclone diurnal cycle of mature hurricanes. *Mon. Wea. Rev.*, **142**, 3900–3919, doi:10.1175/MWR-D-13-00191.1.

Enagonio, J., and M. T. Montgomery, 2001: Tropical cyclogenesis via convectively forced vortex Rossby waves in a shallow water primitive equation model. *J. Atmos. Sci.*, **58**, 685–706, doi:10.1175/1520-0469(2001)058<0685:TCVCFV>2.0.CO;2.

Fierro, A. O., and J. M. Reisner, 2011: High-resolution simulation of the electrification and lightning of Hurricane Rita during the period of rapid intensification. *J. Atmos. Sci.*, **68**, 477–494, doi:10.1175/2010JAS3659.1.

Frank, W. M., and E. A. Ritchie, 2001: Effects of vertical wind shear on the intensity and structure of numerically simulated hurricanes. *Mon. Wea. Rev.*, **129**, 2249–2269, doi:10.1175/1520-0493(2001)129<2249:EOVWSO>2.0.CO;2.

Gray, W. M., 1998: The formation of tropical cyclones. *Meteor. Atmos. Phys.*, **67**, 37–69, doi:10.1007/BF01277501.

Guimond, S. R., G. M. Heymsfield, and F. J. Turk, 2010: Multiscale observations of Hurricane Dennis (2005): The effects of hot towers on rapid intensification. *J. Atmos. Sci.*, **67**, 633–654, doi:10.1175/2009JAS3119.1.

——, ——, P. D. Reasor, and A. C. Didlake Jr., 2016: The rapid intensification of Hurricane Karl (2010): New remote sensing observations of convective bursts from the Global Hawk platform. *J. Atmos. Sci.*, **73**, 3617–3639, doi:10.1175/JAS-D-16-0026.1.

Hack, J. J., and W. H. Schubert, 1986: Nonlinear response of atmospheric vortices to heating by organized cumulus convection. *J. Atmos. Sci.*, **43**, 1559–1573, doi:10.1175/1520-0469(1986)043<1559:NROAVT>2.0.CO;2.

Hazelton, A. T., R. Rogers, and R. E. Hart, 2015: Shear-relative asymmetries in tropical cyclone eyewall slope. *Mon. Wea. Rev.*, **143**, 883–903, doi:10.1175/MWR-D-14-00122.1.

——, ——, and ——, 2017: Analyzing simulated convective bursts in two Atlantic hurricanes. Part I: Bursts formation and development. *Mon. Wea. Rev.*, **145**, 3073–3094, doi:10.1175/MWR-D-16-0267.1.

Heymsfield, G. M., J. B. Halverson, J. Simpson, L. Tian, and T. P. Bui, 2001: ER-2 Doppler radar investigations of the eyewall of Hurricane Bonnie during the Convection and Moisture Experiment-3. *J. Appl. Meteor.*, **40**, 1310–1330, doi:10.1175/1520-0450(2001)040<1310:EDRIOT>2.0.CO;2.

Jiang, H., 2012: The relationship between tropical cyclone intensity change and the strength of inner-core convection. *Mon. Wea. Rev.*, **140**, 1164–1176, doi:10.1175/MWR-D-11-00134.1.

——, and E. M. Ramirez, 2013: Necessary conditions for tropical cyclone rapid intensification as derived from 11 years of TRMM data. *J. Climate*, **26**, 6459–6470, doi:10.1175/JCLI-D-12-00432.1.

Kanada, S., and A. Wada, 2015: Numerical study on the extremely rapid intensification of an intense tropical cyclone: Typhoon Ida (1958). *J. Atmos. Sci.*, **72**, 4194–4217, doi:10.1175/JAS-D-14-0247.1.

Kaplan, J., M. DeMaria, and J. A. Knaff, 2010: A revised tropical cyclone rapid intensification index for the Atlantic and eastern North Pacific basins. *Wea. Forecasting*, **25**, 220–241, doi:10.1175/2009WAF2222280.1.

Kelley, O. A., and J. B. Halverson, 2011: How much tropical cyclone intensification can result from the energy released inside a convective burst? *J. Geophys. Res.*, **116**, D20118, doi:10.1029/2011JD015954.

——, J. Stout, and J. B. Halverson, 2004: Tall precipitation cells in tropical cyclone eyewalls are associated with tropical cyclone intensification. *Geophys. Res. Lett.*, **31**, L24112, doi:10.1029/2004GL021616.

——, ——, and ——, 2005: Hurricane intensification detected by continuously monitoring tall precipitation in the eyewall. *Geophys. Res. Lett.*, **32**, L20819, doi:10.1029/2005GL023583.

Knaff, J. A., and R. M. Zehr, 2007: Reexamination of tropical cyclone pressure–wind relationships. *Wea. Forecasting*, **22**, 71–88, doi:10.1175/WAF965.1.

Kossin, J. P., and W. H. Schubert, 2001: Mesovortices, polygonal flow patterns, and rapid pressure falls in hurricane-like vortices. *J. Atmos. Sci.*, **58**, 2196–2209, doi:10.1175/1520-0469(2001)058<2196:MPFPAR>2.0.CO;2.

——, and M. Sitkowski, 2009: An objective model for identifying secondary eyewall formation in hurricanes. *Mon. Wea. Rev.*, **137**, 876–892, doi:10.1175/2008MWR2701.1.

McFarquhar, G. M., B. F. Jewett, M. S. Gilmore, S. W. Nesbitt, and T. Hsieh, 2012: Vertical velocity and microphysical distributions related to rapid intensification in a simulation of Hurricane Dennis (2005). *J. Atmos. Sci.*, **69**, 3515–3534, doi:10.1175/JAS-D-12-016.1.

Molinari, J., and D. Vollaro, 2014: Symmetric instability in the outflow layer of a major hurricane. *J. Atmos. Sci.*, **71**, 3739–3746, doi:10.1175/JAS-D-14-0117.1.

Möller, J. D., and M. T. Montgomery, 1999: Vortex Rossby waves and hurricane intensification in a barotropic model. *J. Atmos. Sci.*, **56**, 1674–1687, doi:10.1175/1520-0469(1999)056<1674:VRWAHI>2.0.CO;2.

Monette, S. A., C. S. Velden, K. S. Griffin, and C. Rozoff, 2012: Examining trends in satellite-detected tropical overshooting tops as a potential predictor of tropical cyclone rapid intensification. *J. Appl. Meteor. Climatol.*, **51**, 1917–1930, doi:10.1175/JAMC-D-11-0230.1.

Nolan, D. S., Y. Moon, and D. P. Stern, 2007: Tropical cyclone intensification from asymmetric convection: Energetics and efficiency. *J. Atmos. Sci.*, **64**, 3377–3405, doi:10.1175/JAS3988.1.

NRL, 2015: NRL tropical cyclone page. Naval Research Laboratory. [Available online at http://www.nrlmry.navy.mil/TC.html.]

Reasor, P. D., R. Rogers, and S. Lorsolo, 2013: Environmental flow impacts on tropical cyclone structure diagnosed from airborne Doppler radar composites. *Mon. Wea. Rev.*, **141**, 2949–2969, doi:10.1175/MWR-D-12-00334.1.

Rodgers, E. B., W. S. Olson, V. M. Karyampudi, and H. F. Pierce, 1998: Satellite-derived latent heating distribution and environmental influences in Hurricane Opal (1995). *Mon. Wea. Rev.*, **126**, 1229–1247, doi:10.1175/1520-0493(1998)126<1229:SDLHDA>2.0.CO;2.

Rogers, R., 2010: Convective-scale structure and evolution during a high-resolution simulation of tropical cyclone rapid intensification. *J. Atmos. Sci.*, **67**, 44–70, doi:10.1175/2009JAS3122.1.

——, P. Reasor, and S. Lorsolo, 2013: Airborne Doppler observations of the inner-core structural differences between intensifying and steady-state tropical cyclones. *Mon. Wea. Rev.*, **141**, 2970–2991, doi:10.1175/MWR-D-12-00357.1.

——, ——, and J. A. Zhang, 2015: Multiscale structure and evolution of Hurricane Earl (2010) during rapid intensification. *Mon. Wea. Rev.*, **143**, 536–562, doi:10.1175/MWR-D-14-00175.1.

——, J. A. Zhang, J. Zawislak, G. R. Alvey, E. J. Zipser, and H. Jiang, 2016: Observations of the structure and evolution of Hurricane Edouard (2014) during intensity change. Part II: Kinematic structure and the distribution of deep convection. *Mon. Wea. Rev.*, **144**, 3355–3376, doi:10.1175/MWR-D-16-0017.1.

Shay, L. K., G. J. Goni, and P. G. Black, 2000: Effect of a warm ocean ring on Hurricane Opal. *Mon. Wea. Rev.*, **128**, 1366–1383, doi:10.1175/1520-0493(2000)128<1366:EOAWOF>2.0.CO;2.

Smith, R. K., and M. T. Montgomery, 2016: The efficiency of diabatic heating and tropical cyclone intensification. *Quart. J. Roy. Meteor. Soc.*, **142**, 2081–2086, doi:10.1002/qj.2804.

Steranka, J., E. B. Rodgers, and R. C. Gentry, 1986: The relationship between satellite measured convective bursts and tropical cyclone intensification. *Mon. Wea. Rev.*, **114**, 1539–1546, doi:10.1175/1520-0493(1986)114<1539:TRBSMC>2.0.CO;2.

Stern, D. P., and D. S. Nolan, 2012: On the height of the warm core in tropical cyclones. *J. Atmos. Sci.*, **69**, 1657–1680, doi:10.1175/JAS-D-11-010.1.

——, J. R. Brisbois, and D. S. Nolan, 2014: An expanded dataset of hurricane eyewall sizes and slopes. *J. Atmos. Sci.*, **71**, 2747–2762, doi:10.1175/JAS-D-13-0302.1.

Stevenson, S. N., K. L. Corbosiero, and J. Molinari, 2014: The convective evolution and rapid intensification of Hurricane Earl (2010). *Mon. Wea. Rev.*, **142**, 4364–4380, doi:10.1175/MWR-D-14-00078.1.

Susca-Lopata, G., J. Zawislak, E. J. Zipser, and R. F. Rogers, 2015: The role of observed environmental conditions and precipitation evolution in the rapid intensification of Hurricane Earl (2010). *Mon. Wea. Rev.*, **143**, 2207–2223, doi:10.1175/MWR-D-14-00283.1.

Tallapragada, V., C. Kieu, Y. Kwon, S. Trahan, Q. Liu, Z. Zhang, and I. Kwon, 2014: Evaluation of storm structure from the operational HWRF during 2012 implementation. *Mon. Wea. Rev.*, **142**, 4308–4325, doi:10.1175/MWR-D-13-00010.1.

Vigh, J. L., and W. H. Schubert, 2009: Rapid development of the tropical cyclone warm core. *J. Atmos. Sci.*, **66**, 3335–3350, doi:10.1175/2009JAS3092.1.

Willoughby, H. E., 1990: Temporal changes of the primary circulation in tropical cyclones. *J. Atmos. Sci.*, **47**, 242–264, doi:10.1175/1520-0469(1990)047<0242:TCOTPC>2.0.CO;2.

——, J. A. Clos, and M. G. Shoreibah, 1982: Concentric eyewalls, secondary wind maxima, and the evolution of the hurricane vortex. *J. Atmos. Sci.*, **39**, 395–411, doi:10.1175/1520-0469(1982)039<0395:CEWSWM>2.0.CO;2.

Zagrodnik, J. P., and H. Jiang, 2014: Rainfall, convection, and latent heating distributions in rapidly intensifying tropical cyclones. *J. Atmos. Sci.*, **71**, 2789–2809, doi:10.1175/JAS-D-13-0314.1.

Zhuge, X., J. Ming, and Y. Wang, 2015: Reassessing the use of inner-core hot towers to predict tropical cyclone rapid intensification. *Wea. Forecasting*, **30**, 1265–1279, doi:10.1175/WAF-D-15-0024.1.